

**Subject:** Detailed Responses to Reviewers: Liu, H., Maghoul, P., and Shalaby, A.: Seismic physics-based characterization of permafrost sites using surface waves, *The Cryosphere Discuss.* [preprint], <https://doi.org/10.5194/tc-2021-219>, in review, 2021.

**Date:** November 15, 2021

---

The authors are grateful for the valuable comments and kind consideration of our submission. Detailed responses and revisions based on these comments are listed below.

## 1 General Comments

The main contribution of this article is the identification of two wave modes that interact sensitively with the porous and mechanical properties of a layered poro-elastic medium, respectively. In addition the authors use a multiphase poro-mechanical foundation to build a global matrix model of a layered poro-elastic medium. This approach has significant novelty compared to the typical global matrix models based on partial wave amplitudes and nicely emphasizes the connection between surface waves and ground physical properties. The specific application to permafrost demonstrates the relevance of this manuscript to *The Cryosphere*, although certain aspects of the methodology also have broader relevance to the field of near surface geophysics and non-destructive testing of engineering materials.

The weaker side of the manuscript is that findings that are a direct result of the data examples presented are not adequately separated from other applications that remain essentially hypothetical (these are detailed under “specific comments”).

In this paper, our results demonstrate the potential of seismic surface wave testing accompanied with our proposed hybrid inverse and poromechanical dispersion model for the assessment and quantitative characterization of permafrost sites. We have clarified that its applications for early detection and warning systems to monitor infrastructure impacted by permafrost-related geohazards, and to detect the presence of layers vulnerable to permafrost carbon feedback and emission of greenhouse gases into the atmosphere will be the goal of our future studies.

The manuscript could also be improved substantially by giving a more complete description of the two Rayleigh wave modes so that those reading the manuscript may better understand their propagation and interpret their broader relevance to the field of surface wave seismic investigation.

More information of the two Rayleigh wave modes (R1 and R2) is given to better explain their propagation in permafrost foundations (details are given in the answer of Question 15).

Furthermore, I have some concerns that the inversion results are overly sensitive to the frequency range of the dispersion curves that constrain the inversion (likely due to a mismatch between the shape of the experimental and inverted dispersion curves). The anomalous result at 360-480 m in the physical data example is not convincing and appears more likely to reflect a weakness in the

inversion methodology than real lateral variation in physical properties.

In our inversion analysis in the original manuscript, we assumed that the last layer in our model is the unfrozen ground, which is indeed uncertain considering that the penetrating depth is only about 11 m in the MASW survey (based on the recommendation that MASW investigation depth is roughly half of the maximum wavelength (Olafsdottir et al., 2018)). For instance, the maximum wavelength in Section 1 is about 22 m (calculated using a phase velocity of 404 m/s at the frequency of 18 Hz). The maximum wavelength for Section 2 to 5 can be calculated in a similar manner. The average maximum wavelength for the entire investigation areas is around 21 m. Therefore, the penetrating depth in the MASW survey presented in this study is only about 11 m. It was reported that the permafrost layer in the studied site can go up to 100 m (Dolnicki et al., 2013; Glazer et al., 2018). Therefore, in the revised paper, we considered the last layer to have a degree of saturation of unfrozen water ranging from 1% to 99%. In this way, the last layer can be either permafrost or unfrozen ground. We have also applied the automatic methods for the selection of dispersion curves (instead of relying on visual inspection that we used in the original draft) using MASWave software (Olafsdottir, 2018). The misfits (RMS) between the R1 experimental and numerical dispersion curves at Section 4 have been significantly reduced from 49.6 to only 4.7 , as shown in Figure 1g.

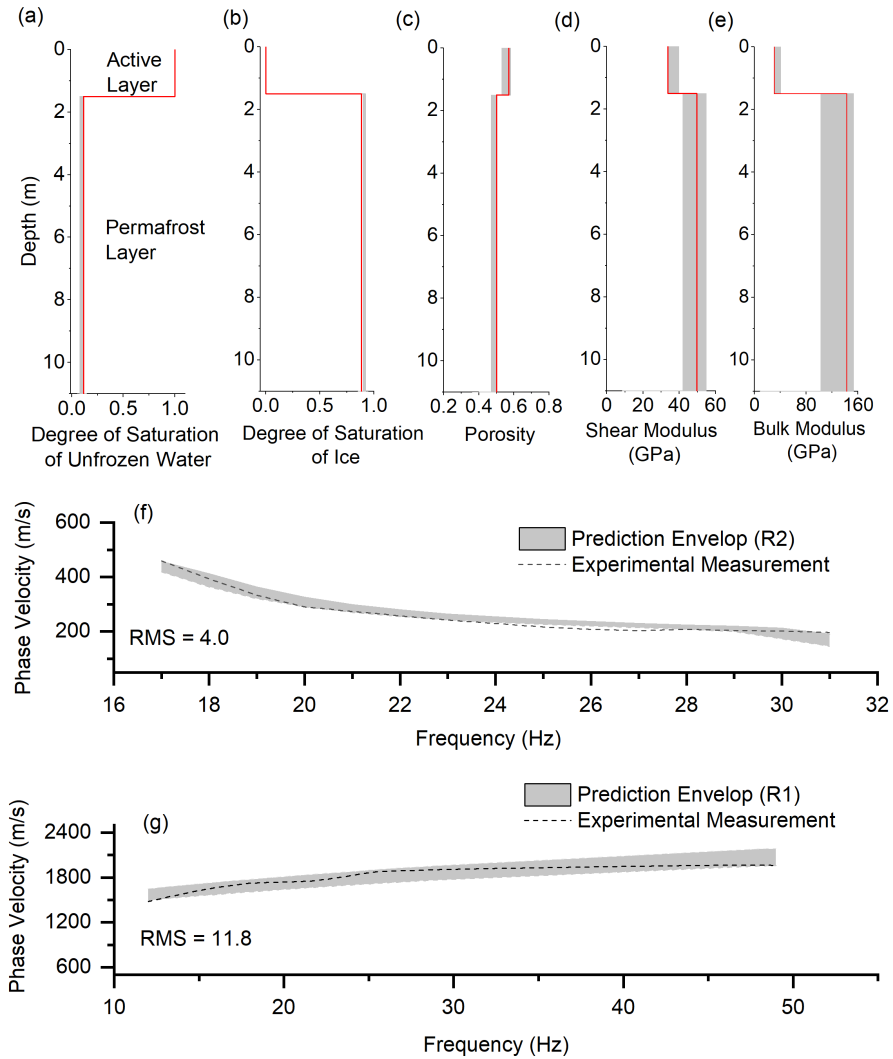


Figure 1: Surface wave inversion results for Section 4 (from 360m to 480m). **(a)** Degree of saturation of unfrozen water, **(b)** Degree of saturation of ice, **(c)** Porosity distribution, **(d)** Shear modulus of solid skeletal frame, **(e)** Bulk modulus of solid skeletal frame, **(f)** Experimental and numerical dispersion curves for R2 wave, **(g)** Experimental and numerical dispersion curves for R1 wave.

Furthermore, it is generally difficult to assess the true accuracy of the results owing to a lack of comparison to ground truth observations of physical properties and interface depths or comparison with other geophysical datasets (both of which appear to exist in the published literature). I believe it should be possible for the authors to address these concerns in a revised manuscript, that will then make a useful contribution to The Cryosphere.

In the revised manuscript, the comparison of the inversion results using the proposed hybrid inverse and multi-phase poro-mechanical approach and inversion results from ERT survey provided by Glazer et al., (2020) has been added. It was reported by Glazer et al., (2020) that the permafrost table is located at a depth of about 2 m for a span of 20 m. The new inversion results in terms of

the thickness of the active layer were also validated using the results reported by Dobiński et al., (2010) and Dolnicki et al., (2013) by the direct probing method. It was also reported by Dobiński et al., (2010) and Dolnicki et al., (2013) that the active layer in Svalbard is approximately 1.65–2.5 m deep. The direct sampling results reported by Szymański et al. (2013) confirmed that the study site is very wet and the water table is very high (around 15 cm). It was reported by Szymański et al. (2013) that this study site also contains a lot of coarse sandy soils, gravels as well as around 20% silty clay based on the direct sampling methods at the top 15 cm. Our inversion results, as shown in Figure 2, predicted that the permafrost table is generally located at about 1.5-1.9 m below the ground surface, which is consistent with the ERT results reported by Glazer et al., (2020) and results reported by Dobiński et al., (2010) and Dolnicki et al., (2013) using the direct probing method.

Based on the field description of the testing site by Glazer et al., (2020), the unconsolidated sedimentary rock contains a high proportion of pore spaces; consequently, they can accumulate a large volume of pore-water or pore-ice. Our inversion results showed that the porosity of the active layer ranges from 0.56 to 0.69, which is consistent with the field description by Glazer et al., (2020). The unfrozen water content in the second permafrost layer was predicted ranging from 0.05-0.17. Li et al. (2020) and Zhang et al. (2020) showed that the residual volumetric unfrozen water content for silty-clay, clay, medium sand, and fine sand is 0.12, 0.08, 0.06 and 0.03, respectively. Our inversion results predicted that soils are mostly silty-clay or clay (Section 1-3) and sandy soils, which are also consistent with the results described by Szymański et al. (2013). Figure 2e shows the variation of the shear modulus of soil skeleton predicted by the proposed hybrid inverse and multi-phase poro-mechanical approach. The predicted shear modulus in the first layer at the offset distance of 0 to 360 m ranges from 4 GPa to 7.9 GPa, which represents clay soils (Helgerud ET AL. 1999). At the offset distance of 360 to 600 m, the estimated shear modulus in the first layer ranges from 27 GPa to 33 GPa, which corresponds to soils with calcite constituents (Helgerud ET AL. 1999). Calcite most commonly occurs in sedimentary rock or gravels (Schmid et al., 1987), which is consistent with the field description given by Glazer et al. 2020 and Szymański et al. (2013).

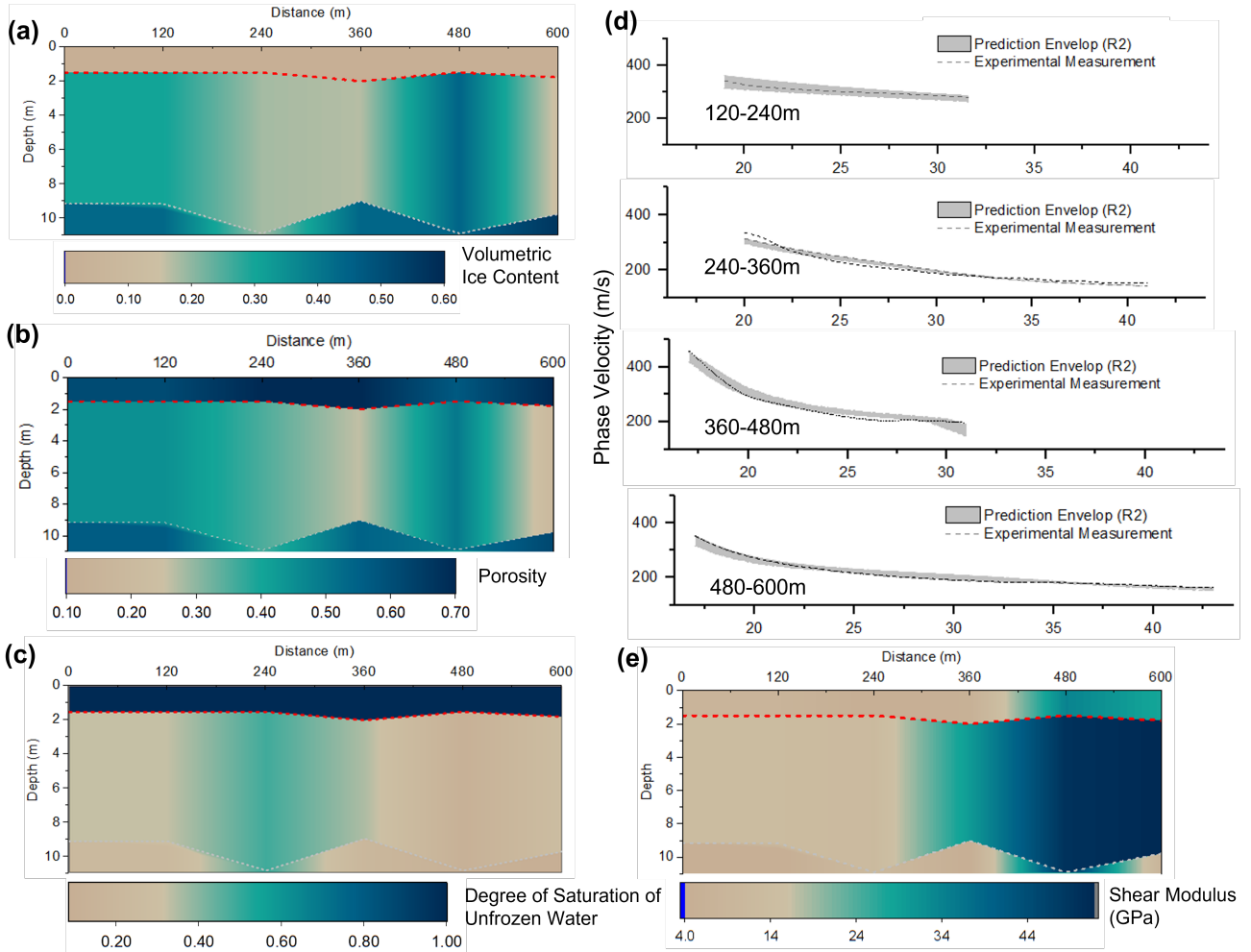


Figure 2: Summary of the inversion results at the offset distance from 0 m to 600 m. **(a)** Volumetric ice content distribution. **(b)** Soil porosity distribution. **(c)** Distribution of the degree saturation of unfrozen water. **(d)** Comparison between the numerical and experimental dispersion curves for R2 wave. **(e)** Distribution of the shear modulus of the solid skeletal frame.

Reference:

Glazer, M., Dobiński, W., Marciniak, A., Majdański, M., & Błaszczuk, M. (2020). Spatial distribution and controls of permafrost development in non-glacial Arctic catchment over the Holocene, Fuglebekken, SW Spitsbergen. *Geomorphology*, 358, 107128.

Szymański, W., Skiba, S., & Wojtuń, B. (2013). Distribution, genesis, and properties of Arctic soils: a case study from the Fuglebekken catchment, Spitsbergen. *Polish Polar Research*, 289-304.

Helgerud, M. B., Dvorkin, J., Nur, A., Sakai, A., & Collett, T. (1999). Elastic-wave velocity in marine sediments with gas hydrates: Effective medium modeling. *Geophysical Research Letters*, 26(13), 2021-2024.

Li, Z., Chen, J., & Sugimoto, M. (2020). Pulsed NMR measurements of unfrozen water content in

partially frozen soil. *Journal of Cold Regions Engineering*, 34(3), 04020013.

Zhang, M., Zhang, X., Lai, Y., Lu, J., & Wang, C. (2020). Variations of the temperatures and volumetric unfrozen water contents of fine-grained soils during a freezing–thawing process. *Acta Geotechnica*, 15(3), 595-601.

Dolnicki, P., Grabiec, M., Puczko, D., Gawor, L., Budzik, T., & Klementowski, J. (2013). Variability of temperature and thickness of permafrost active layer at coastal sites of Svalbard.

Dobiński, W., & Leszkiewicz, J. (2010). Active layer and permafrost occurrence in the vicinity of the Polish Polar Station, Hornsund, Spitsbergen in the light of geophysical research. *Problemy Klimatologii Polarnej*, 20, 129-142.

Olafsdottir, E. A., Erlingsson, S., & Bessason, B. (2018). Tool for analysis of multichannel analysis of surface waves (MASW) field data and evaluation of shear wave velocity profiles of soils. *Canadian Geotechnical Journal*, 55(2), 217-233.

## 2 Specific comments

1. The authors claim that their methodology can be used to “characterize a permafrost site more accurately” (line 12). However, since we have no baseline for comparison it is difficult to assess to what extent this is the case. The Glazer (2020) study that is already cited by the authors could be used as a direct comparison in order to place the results of the present study in context. The ERT results of Glazer (2020) may provide a means of independent validation, while the MASW results of Glazer (2020) use more conventional processing of the same dataset as used in this study and could provide an excellent benchmark to highlight the benefits of the new hybrid inversion approach.

Szymański et al. (2013) have published direct sampling results of 34 soil pits for the Fuglebekken area. It would be highly valuable for the authors to refer to this study in order to place their results in a geological context. Significantly, Szymański et al. (2013) describe the area as consisting of crystalline bedrock covered by marine deposits with thickness up to 4-5 m. Is there a possibility that the interface between the active layer and the ice bearing permafrost that the authors place at 4 m depth is really the sediment-bedrock interface?

In the revised manuscript, the comparison of the inversion results using the proposed hybrid inverse and multi-phase poro-mechanical approach and inversion results from ERT survey provided by Glazer et al., (2020) has been added. It was reported by Glazer et al., (2020) that the permafrost table is located at a depth of about 2 m for a span of 20 m. The new inversion results in terms of the thickness of the active layer were also validated using the results reported by Dobiński et al., (2010) and Dolnicki et al., (2013) by the direct probing method. It was also reported by Dobiński et al., (2010) and Dolnicki et al., (2013) that the active layer in Svalbard is approximately 1.65–2.5 m deep. The direct sampling results reported by Szymański et al. (2013) confirmed that the study site is very wet and the water table is very high (around 15 cm). It was reported by Szymański et al. (2013) that this study site also contains a lot of coarse sandy soils, gravels as well as around 20% silty clay based on the direct sampling methods at the top 15 cm. Our inversion results, as shown in Figure 2, predicted that the permafrost table is generally located at about 1.5-1.9 m below the ground surface, which is consistent with the ERT results reported by Glazer et al., (2020) and results reported by Dobiński et al., (2010) and Dolnicki et al., (2013) using the direct probing method.

Based on the field description of the testing site by Glazer et al., (2020), the unconsolidated sedimentary rock contains a high proportion of pore spaces; consequently, they can accumulate a large volume of pore-water or pore-ice. Our inversion results showed that the porosity of the active layer ranges from 0.56 to 0.69, which is consistent with the field description by Glazer et al., (2020). The unfrozen water content in the second permafrost layer was predicted ranging from 0.05-0.17. Li et al. (2020) and Zhang et al. (2020) showed that the residual volumetric unfrozen water content for silty-clay, clay, medium sand, and fine sand is 0.12, 0.08, 0.06 and 0.03, respectively. Our inversion results predicted that soils are mostly silty-clay or clay (Section 1-3) and sandy soils, which are also consistent with the results described by Szymański et al. (2013). Figure 2e shows the variation of the shear modulus of soil skeleton predicted by the proposed hybrid inverse and multi-phase poro-mechanical approach. The predicted shear modulus in the first layer at the offset distance of 0 to 360 m ranges from 4 GPa to 7.9 GPa, which represents clay soils (Helgerud ET AL. 1999). At the offset distance of 360 to 600 m, the estimated shear modulus in the first layer ranges from 27 GPa to 33 GPa, which corresponds to soils with calcite constituents (Helgerud ET AL. 1999). Calcite most commonly occurs in sedimentary rock or gravels (Schmid et al., 1987),

which is consistent with the field description given by Glazer et al. 2020 and Szymański et al. (2013).

Glazer et al. (2020) reported that at the studied site, the marine deposits reaching up to 15 m below ground level. Since we only focus on the investigation depth of the top 11 m in this paper (based on the recommendation that MASW investigation depth is roughly half of the maximum wavelength (Olafsdottir et al., 2018)), it is very unlikely that we can see the bedrock in our inversion results.

Reference:

Glazer, M., Dobiński, W., Marciniak, A., Majdański, M., & Błaszczuk, M. (2020). Spatial distribution and controls of permafrost development in non-glacial Arctic catchment over the Holocene, Fuglebekken, SW Spitsbergen. *Geomorphology*, 358, 107128.

Szymański, W., Skiba, S., & Wojtuń, B. (2013). Distribution, genesis, and properties of Arctic soils: a case study from the Fuglebekken catchment, Spitsbergen. *Polish Polar Research*, 289-304.

Li, Z., Chen, J., & Sugimoto, M. (2020). Pulsed NMR measurements of unfrozen water content in partially frozen soil. *Journal of Cold Regions Engineering*, 34(3), 04020013.

Zhang, M., Zhang, X., Lai, Y., Lu, J., & Wang, C. (2020). Variations of the temperatures and volumetric unfrozen water contents of fine-grained soils during a freezing–thawing process. *Acta Geotechnica*, 15(3), 595-601.

Helgerud, M. B., Dvorkin, J., Nur, A., Sakai, A., & Collett, T. (1999). Elastic-wave velocity in marine sediments with gas hydrates: Effective medium modeling. *Geophysical Research Letters*, 26(13), 2021-2024.

Carcione, J. M., & Seriani, G. (2001). Wave simulation in frozen porous media. *Journal of Computational Physics*, 170(2), 676-695.

Schmid, S. M., Panozzo, R., & Bauer, S. (1987). Simple shear experiments on calcite rocks: rheology and microfabric. *Journal of structural Geology*, 9(5-6), 747-778.

2. The dispersion spectra for the R2 wave (Fig. 1b) looks very similar to the Rayleigh-Lamb waves described by Ryden & Park (2004) for pavements and also shown to occur in permafrost settings by Romeyn et al. (2021), although the experimental data in the present study does not resolve the higher order modes. It would be beneficial for the authors to refer to this work, particularly since the global matrix method employed by Ryden & Park (2004) is similar to the theoretical development of this manuscript. It may be purely an issue of terminology, but the authors could also consider that the surface waves identified in the manuscript may be more accurately considered Rayleigh-Lamb waves, since the stiff ice-bearing permafrost layer likely acts as a waveguide to some extent. The following passage from Ryden & Park (2004) provides some perspective on this topic:

“It is usually assumed that Rayleigh waves are the prevailing type of waves generated, with a depth penetration of about one wavelength (Viktorov 1967). However, it has been reported that this assumption holds strictly only at sites where the stiffness increases smoothly as a function of

depth (Foti 2000). At sites with a velocity reversal (i.e. stiffness decreases with depth), the nature of surface-wave propagation has been reported as more complicated than at sites with normal dispersion. Several studies have indicated that a measured dispersion curve where the phase velocity increases with frequency, i.e. inverse dispersion, is actually built up by small portions of higher modes (Gucunski and Woods 1992; Tokimatzu et al. 1992; Forbriger 2003; Foti et al. 2003; Ryden et al. 2004)."

The Rayleigh-Lamb waves are formed by interference of multiple reflections and mode conversion of compressional waves (P-waves) and shear waves (S-waves) at the two free boundaries of the plate. Strictly speaking, Lamb's theory for these guided waves requires the surfaces of the plate to be traction-free, that is to say the plate should be in a vacuum (Lowe 2001). For pavement structure studied by Ryden & Park (2004), they concluded: 'Lamb-wave dispersion curves for a free plate in a vacuum can represent the reality sufficiently closely only if the stiffness contrast between the top layer and the underlying half-space is large. The resulting error in phase velocity in this case was investigated. It was concluded that the error in phase velocity does not exceed 5% if the fundamental antisymmetric Lamb-wave dispersion curve is used as an approximate theoretical dispersion curve, with the restriction that the shear-wave velocity of the stiff layer is greater than the compressional-wave velocity in the underlying media". For the wave propagation in permafrost, the condition that the shear-wave velocity of the stiff layer (first layer) is greater than the compressional-wave velocity in the underlying media can not be fulfilled.

As mentioned earlier, the formation of guided waves requires multiple reflections and mode conversion of compressional waves (P-waves) and shear waves (S-waves). In the original seismic measurements shown in Figure 3e, we can not see any reflection that can be easily seen in any traditional seismic reflection investigations (e.g., French 1975; Zhao et al., 1993; Symes 2009).

Additionally, the phase velocity of R1 and R2 does not converge to the same velocity as the Rayleigh-Lamb waves do since the generation of R1 or R2 as well as symmetric modes or anti-symmetric modes are very different. The fundamental anti-symmetric mode (A0) and symmetric mode (S0) of Rayleigh-Lamb waves tend to converge to the same phase velocity (as described by Ryden & Park (2004)). The symmetric modes, also called longitudinal modes, are generated due to the wave propagation in the longitudinal direction. On the other hand, the antisymmetric modes are generated because of the wave propagation in the transverse direction (Graff 2012). The generation of R1 and R2 is due to the interaction of multiphase components (soil skeleton, unfrozen water and ice). We have proved that R1 waves appear due to the interaction of P1 and S1 waves. Similarly, R2 waves appear due to the interaction of P2 and S2 waves. However, the generation of anti-symmetric mode and symmetric mode is due to the geometry that constrains the wave propagation. The anti-symmetric mode and symmetric mode can be seen in solid materials. However, the R1 and R2 can only be generated in frozen soils with at least three phases.

For the dispersion curve of R1 mode, it is very different from the dispersion curve build up from the higher mode. If the dispersion curve is built up by small portions of higher modes, we can easily see the cutting off frequency (as shown by Romeyn et al., 2021 in Figure 7 in their manuscript). This is not the case for the dispersion curve shown in Figure 3f in our study.

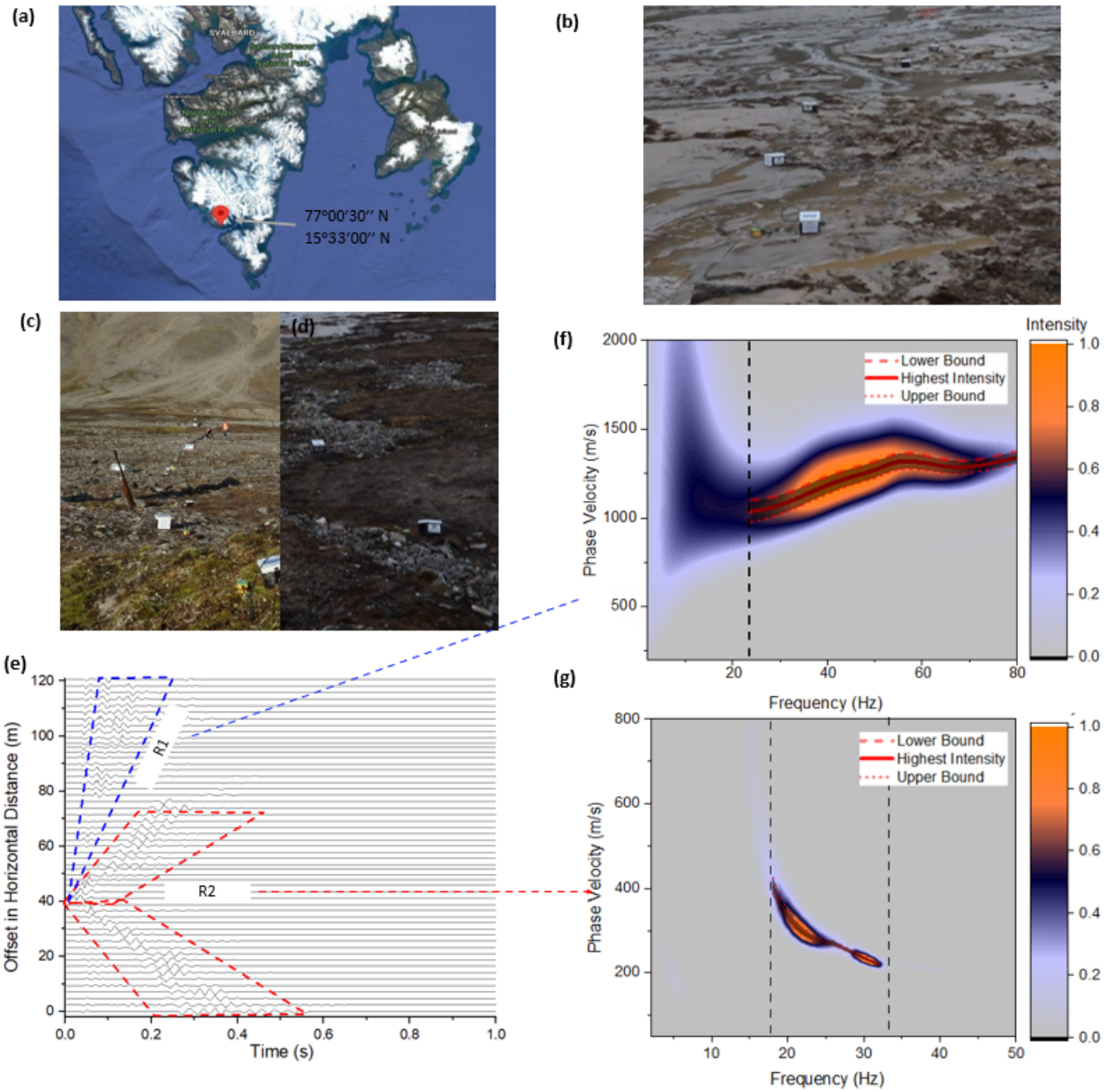


Figure 3: Surface wave measurement in Section 1 (from 0 m to 120 m). **(a)** Study area in Holocene, Fuglebekken, SW Spitsbergen. **(b)** Test site with clayey silt soils. **(c)** Test site with gravels and sands. **(d)** Test site with patterned ground. **(e)** Waveform data from the measurements at different offsets in horizontal distance. **(f)** Experimental dispersion image for R1 wave. **(g)** Experimental dispersion image for R2 wave.

Reference:

Rydén, N., & Park, C. B. (2004). Surface waves in inversely dispersive media. *Near surface geophysics*, 2(4), 187-197.

Graff, K. F. (2012). *Wave motion in elastic solids*. Courier Corporation.

Romeyn, R., Hanssen, A., Ruud, B. O., Stemland, H. M., & Johansen, T. A. (2021). Passive seismic recording of cryoseisms in Adventdalen, Svalbard. *The Cryosphere*, 15(1), 283-302.

M.J.S. Lowe, *Wave propagation — Guided Waves in Structures*. Encyclopedia of Vibration, Elsevier, 2001, Pages 1551-1559, ISBN 9780122270857, <https://doi.org/10.1006/rwvb.2001.0173>.

Symes, W. W. (2009). The seismic reflection inverse problem. *Inverse problems*, 25(12), 123008.

Zhao, W., Nelson, K. D., Che, J., Quo, J., Lu, D., Wu, C., & Liu, X. (1993). Deep seismic reflection evidence for continental underthrusting beneath southern Tibet. *Nature*, 366(6455), 557-559.

French, W. S. (1975). Computer migration of oblique seismic reflection profiles. *Geophysics*, 40(6), 961-980.

3. The proposed application in “early detection and warning systems to monitor infrastructure impacted by permafrost-related geohazards” (line 12) is not sufficiently developed. It should be established by data, reference to other studies or at least step-by-step logic that precursor change in physical properties could be detected by the proposed monitoring methodology in advance of changes that result in structural damage, for example. If such evidence does not exist, this application should be limited to a briefly describing that this early detection system is a goal that will be pursued in future studies.

In the revised manuscript, we have clarified that the development of the early warning system for the long-term tracking of permafrost conditions will be the goal of our future study. In the early warning system, the amount the ice content within permafrost can be used as a key parameter to indicate the state of permafrost. The thawing permafrost is a continuous process in which the temperature of permafrost gradually increases (ice content gradually decreases). In the future study, we will focus on the development of an early warning system for the long-term tracking of permafrost conditions. The early warning system can be used to collect seismic measurements and predict the physical and mechanical properties of the foundation permafrost. The system then reports periodic variations in physical (mostly ice content) and mechanical properties of the permafrost being monitored. The same method being applied on different dates (e.g. seasonal basis) can be used to record the change of properties of the permafrost site, and then warn on the degradation of the permafrost exceeding the threshold. The value of the threshold (or critical values) will require more in-depth research to be determined.

4. The possibility to “detect the presence of layers vulnerable to permafrost carbon feedback and emission of greenhouse gases into the atmosphere” (line 13) is not convincingly demonstrated and may overemphasize the direct relevance of this study to assessment of the global carbon budget. If one reads carefully through the manuscript, this statement comes down to the hypothesized ability of the study methodology to detect the presence of peat in the subsurface. The authors have not argued how distinct the physical parameters of peat are from other soil types and to what level of confidence it could be detected in practice. Ideally, there should be at least one real data example of a known peat layer being detected by proposed methodology. Synthetic data could also be usefully employed to demonstrate the hypothesized application. I would further suggest that the authors describe specifically that there are two steps, 1) detection of peat layers 2) estimation of carbon content. It should otherwise be clearly demonstrated that the variation of organic carbon content of soils that are otherwise similar leads to a detectable variation in mechanical properties

using Rayleigh wave modes 1 & 2.

We have clarified the application of early detection and warning systems to detect the presence of layers vulnerable to permafrost carbon feedback and emission of greenhouse gases into the atmosphere will be the goal of future study. However, its applications for early detection and warning systems to monitor infrastructure impacted by permafrost-related geohazards, and to detect the presence of layers vulnerable to permafrost carbon feedback and emission of greenhouse gases into the atmosphere are provided with more details. Currently, there is no advanced physics-based monitoring system developed for the real-time interpretation of seismic measurements. As such, active and passive seismic measurements can be collected and processed using the proposed hybrid inverse and poromechanical dispersion model for the assessment and quantitative characterization of permafrost sites at various depths in real-time. In the future study, we will focus on the development of an early warning system for the long-term tracking of permafrost conditions. The early warning system can be used to collect seismic measurements and predict the physical and mechanical properties of the foundation permafrost. The system then reports periodic variations in physical (mostly ice content) and mechanical properties of the permafrost being monitored. The same method being applied on different dates (e.g. seasonal basis) can be used to record the change of properties of the permafrost site, and then warn on the degradation of the permafrost exceeding the threshold. The value of the threshold (or critical values) will require more in-depth research to be determined. The early detection and warning systems can be beneficial in monitoring the condition of the foundation permafrost and preventing excessive thawing settlement and significant loss in strength. Similarly, we can detect the presence of peat (based on the physical and mechanical properties) which is vulnerable to permafrost carbon feedback and emission of greenhouse gases into the atmosphere. It's reported that the soils in the permafrost region hold twice as much carbon as the atmosphere does (almost 1,600 billion tonnes) (Schuur et al., 2015). The thawing permafrost can rapidly trigger landslides and erosion. Current climate models assume that permafrost thaws gradually from the surface downwards (Schuur et al., 2015). However, several meters of soil can become destabilized within a few days or weeks instead of a few centimeters of soil thawing each year (Schuur et al., 2015). The missing element of the existing studies and models is that the abrupt permafrost destabilization can occur and contribute to more carbon feedback than the existing models predict as the permafrost degrades.

Reference:

Schuur, E. A., McGuire, A. D., Schädel, C., Grosse, G., Harden, J. W., Hayes, D. J., & Vonk, J. E. (2015). Climate change and the permafrost carbon feedback. *Nature*, 520(7546), 171-179.

5. Line 16-19. Missing reference. In particular "The thickness of the active layer depends on local geological and climate conditions such as vegetation, soil composition, air temperature, solar radiation and wind speed" should be supported with one or more references. The active layer undergoes seasonal freeze and thaw cycles by definition so to say "may undergo" seems strange (I assume this was an oversight and have added a technical correction).

References have been added. Permafrost is defined as the ground that remains at or below 0 °C for at least two consecutive years (Riseborough et al., 2008). The shallower layer of the ground in permafrost areas, termed as the active layer, undergoes seasonal freeze-thawing cycles (Shur Y., 2011). The thickness of the active layer depends on local geological and climate conditions such as vegetation, soil composition, air temperature, solar radiation and wind speed (Liu et al., 2019b).

Also, we have removed the 'may' in the sentence.

Reference:

Riseborough, D., Shiklomanov, N., Etzelmüller, B., Gruber, S., & Marchenko, S. (2008). Recent advances in permafrost modelling. *Permafrost and Periglacial Processes*, 19(2), 137-156.

Shur Y., Jorgenson M.T., Kanevskiy M.Z. (2011). Permafrost. In: Singh V.P., Singh P., Haritashya U.K. (eds) *Encyclopedia of Snow, Ice and Glaciers*. *Encyclopedia of Earth Sciences Series*.

Liu, H., Maghoul, P., Shalaby, A., & Bahari, A. (2019). Thermo-hydro-mechanical modeling of frost heave using the theory of poroelasticity for frost-susceptible soils in double-barrel culvert sites. *Transportation Geotechnics*, 20, 100251.

**6. Line 24. Missing reference. Please add one or more references that support the excessive deformation in frost-susceptible soils caused by segregated ice formation.**

Reference has been added. Segregated ice is formed when water migrates to the freezing front and it can cause excessive deformations in frost-susceptible soils (Liu et al., 2019a, b).

Reference:

Liu, H., Maghoul, P., & Shalaby, A. (2019). Optimum insulation design for buried utilities subject to frost action in cold regions using the Nelder-Mead algorithm. *International Journal of Heat and Mass Transfer*, 130, 613-639.

Liu, H., Maghoul, P., Shalaby, A., & Bahari, A. (2019). Thermo-hydro-mechanical modeling of frost heave using the theory of poroelasticity for frost-susceptible soils in double-barrel culvert sites. *Transportation Geotechnics*, 20, 100251.

**7. Line 27. Missing reference. Please add one or more references that describe the ice-wedge formation process and its timescale.**

Reference has been added. Ice wedges are large masses of ice formed over many centuries by repeated frost cracking and ice vein growth (Harry et al. 1998).

Reference:

Harry, D. G., & Gozdzik, J. S. (1988). Ice wedges: growth, thaw transformation, and palaeoenvironmental significance. *Journal of Quaternary Science*, 3(1), 39-55.

**8. Line 33. Missing reference. Please add one or more references that describe thaw settlement and associated loss of strength.**

Reference has been added. The construction on thaw-unstable permafrost is challenging and requires remedial measures since upon thawing, permafrost will experience significant thaw-settlement and suffer loss of strength to values significantly lower than that for similar material in

an unfrozen state (Buteau et al. 2010; Liu et al. 2019).

Reference:

Buteau, S., Fortier, R., & Allard, M. (2010). Permafrost weakening as a potential impact of climatic warming. *Journal of Cold Regions Engineering*, 24(1), 1-18.

Liu, H., Maghoul, P., Shalaby, A., & Bahari, A. (2019). Thermo-hydro-mechanical modeling of frost heave using the theory of poroelasticity for frost-susceptible soils in double-barrel culvert sites. *Transportation Geotechnics*, 20, 100251.

**9. Line 56. Missing reference. It is stated that it is common practice to associate anomalously high shear wave velocities with permafrost, but no references are given to studies that are examples of this practice.**

Reference has been added. It is commonly considered that the permafrost layer (frozen soil) is associated with a higher shear wave velocity due to the presence of ice in comparison to unfrozen ground (Dou et al, 2014, Glazer et al, 2020).

Reference:

Dou, S., & Ajo-Franklin, J. B. (2014). Full-wavefield inversion of surface waves for mapping embedded low-velocity zones in permafrost. *Geophysics*, 79(6), EN107-EN124.

Glazer, M., Dobiński, W., Marciniak, A., Majdański, M., & Błaszczuk, M. (2020). Spatial distribution and controls of permafrost development in non-glacial Arctic catchment over the Holocene, Fuglebekken, SW Spitsbergen. *Geomorphology*, 358, 107128.

**10. Line 64. Similar to point 3. It is not sufficiently clear what the authors mean by “we can also predict the soil type and the sensitivity of the permafrost layer to permafrost carbon feedback and emission of greenhouse gases to the atmosphere”. It seems natural to guess that this means the ability to quantify the amount of organic carbon present in the soil, but it is not clear to what extent the proposed methodology is capable of this.**

We have clarified the application of early detection and warning systems to detect the presence of layers vulnerable to permafrost carbon feedback and emission of greenhouse gases into the atmosphere will be the goal of future study. In our paper, we have demonstrated that the soil type can be estimated based on the predicted physical and mechanical properties. For instance, the unfrozen water content in the second permafrost layer was predicted ranging from 0.05-0.17. Li et al. (2020) and Zhang et al. (2020) showed that the residual volumetric unfrozen water content for silty-clay, clay, medium sand, and fine sand is 0.12, 0.08, 0.06 and 0.03, respectively. Our inversion results predicted that soils are mostly silty-clay or clay (Section 1-3) and sandy soils, which are also consistent with the results described by Szymański et al. (2013). Figure 2e shows the variation of the shear modulus of soil skeleton predicted by the proposed hybrid inverse and multi-phase poro-mechanical approach. The predicted shear modulus in the first layer at the offset distance of 0 to 360 m ranges from 4 GPa to 7.9 GPa, which represents clay soils (Helgerud ET AL. 1999). At the offset distance of 360 to 600 m, the estimated shear modulus in the first layer ranges from 27 GPa to 33 GPa, which corresponds to soils with calcite constituents (Helgerud et al. 1999). Calcite

most commonly occurs in sedimentary rock or gravels (Schmid et al., 1987), which is consistent with the field description given by Glazer et al. 2020 and Szymański et al. (2013). The prediction of the sensitivity of the permafrost layer to permafrost carbon feedback and emission of greenhouse gases to the atmosphere requires the detection of the peat permafrost layer. This can be done based on the predicted physical and mechanical properties as a preliminary assessment. The mechanical properties of peat are expected to be significantly lower than these of other soil types and our proposed physics-based solver is able to determine the presence of such soils. However, this application still requires in-depth investigation and research.

Reference:

Li, Z., Chen, J., & Sugimoto, M. (2020). Pulsed NMR measurements of unfrozen water content in partially frozen soil. *Journal of Cold Regions Engineering*, 34(3), 04020013.

Zhang, M., Zhang, X., Lai, Y., Lu, J., & Wang, C. (2020). Variations of the temperatures and volumetric unfrozen water contents of fine-grained soils during a freezing–thawing process. *Acta Geotechnica*, 15(3), 595-601.

Szymański, W., Skiba, S., & Wojtuń, B. (2013). Distribution, genesis, and properties of Arctic soils: a case study from the Fuglebekken catchment, Spitsbergen. *Polish Polar Research*, 289-304.

Helgerud, M. B., Dvorkin, J., Nur, A., Sakai, A., & Collett, T. (1999). Elastic-wave velocity in marine sediments with gas hydrates: Effective medium modeling. *Geophysical Research Letters*, 26(13), 2021-2024.

Glazer, M., Dobiński, W., Marciniak, A., Majdański, M., & Błaszczuk, M. (2020). Spatial distribution and controls of permafrost development in non-glacial Arctic catchment over the Holocene, Fuglebekken, SW Spitsbergen. *Geomorphology*, 358, 107128.

**11.** Figure 2. The layer stiffness matrices should be defined in the caption. Perhaps this figure should be dropped entirely since it is minimally illustrative when the layer matrices are only given in the appendices.

We have placed it in the appendix.

**12.** Line 108. “The global stiffness matrix for the R1 wave can be decomposed into the components related only to the P1 and S1 wave velocities.” There should be a reference to an equation associated with this statement.

We have clarified this in the revised manuscript. We have proved that the R1 wave is generated by the interaction between the P1 and S1 waves based on our case study and the characteristic of Rayleigh waves. In our case study shown in Section 3 in the manuscript, the velocities of the P1 and P2 waves are calculated as 2,628 m/s and 910 m/s, respectively, based on the relations given in Appendix A in the manuscript. Similarly, the velocities of the S1 and S2 waves are calculated as 1,217 m/s and 481 m/s, respectively. We also found the velocity of R1 and R2 is 1,150 m/s and 450 m/s using the three-phase dispersion relation derived in this paper (Equation 1). It is known that the Rayleigh wave is slightly slower than the shear wave velocity and the ratio of the Rayleigh wave and shear wave velocity ranges from 0.92-0.95 for the Poisson ratio greater than

0.3 (Kazemirad et al., 2013). From this analysis, we found the ratio of R1 and S1 wave velocity is around 0.93. Similarly, the ratio of R2 and S2 wave velocity is around 0.94. Therefore, we can conclude that R1 waves appear due to the interaction of P1 and S1 waves since the phase velocity of R1 waves is slightly slower than the phase velocity of S1 waves. Similarly, R2 waves appear due to the interaction of P2 and S2 waves since the phase velocity of R2 waves is also slightly slower than the phase velocity of S2 waves. As shown in Figure 5b, the R1 and R2 wave have a much larger amplitude than any other components (e.g., P1, P2, S1 and S2), which is the characteristic of Rayleigh waves. Therefore, the stiffness matrix for R1 wave can be decomposed into the components related only to the P1 and S1 wave velocities.

To further explain this statement, we have shown a dispersion image obtained from the three-phase poro-mechanical approach for a three-layer system. We assumed that the porosity is 0.5 for all three layers; the degree of saturation degree of unfrozen water is 0.1, 0.3 and 0.6, respectively; the shear modulus of soil skeleton is 6.85 GPa, 10 GPa and 10 GPa, respectively; the bulk modulus of soil skeleton is 15 GPa, 15 GPa and 21 GPa, respectively. The image contains two colors (red and blue). The interface of two colors indicates the sign switching of determinant value, which is the definition of dispersion relation. Figure 4a shows the dispersion image (a combination for R1 and R2 waves) calculated using the proposed three-phase poro-mechanical approach. Figure 4b shows the dispersion image using the components related only to the P1 and S1 wave velocities. Figure 4c shows the dispersion image using the components related only to the P2 and S2 wave velocities. Therefore, we can conclude that the global stiffness matrix for the R1 wave can be decomposed into the components related only to the P1 and S1 wave velocities. This approach avoids the difficulties in differentiating the higher modes of R2 wave from the fundamental mode of the R1 wave. The code to generate the results shown in Figure 4 can also be found in our Github repository.

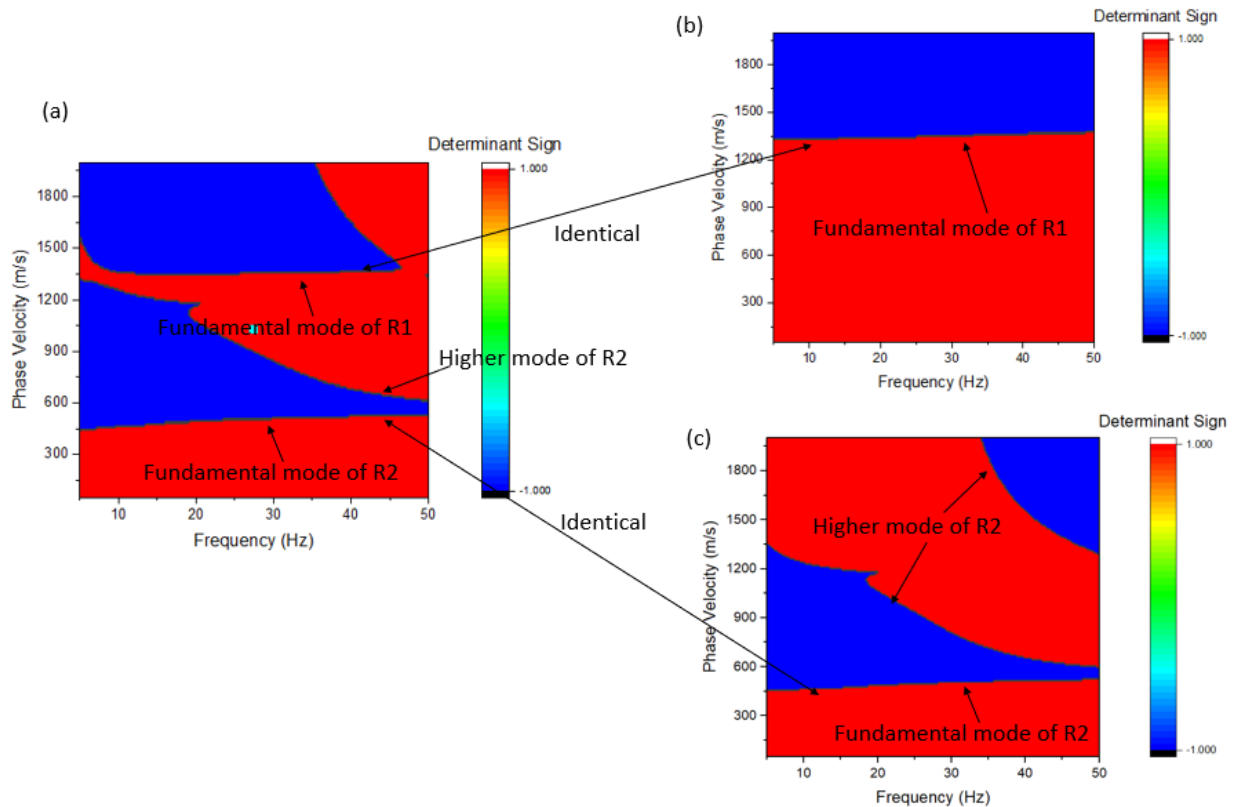


Figure 4: (a) Dispersion image (a combination for R1 and R2 waves) (b) Dispersion image using the components related only to the P1 and S1 wave velocities. (c) Dispersion image using the components related only to the P2 and S2 wave velocities.

Reference:

Kazemirad, S., & Mongeau, L. (2013). Rayleigh wave propagation method for the characterization of a thin layer of biomaterials. *The Journal of the Acoustical Society of America*, 133(6), 4332-4342.

13. Line 109. “proved that the R1 wave is generated by the interaction between the P1 and S1 waves.” Include a reference to section 3 where this argument is made so that the reader does not get lost here.

We have proved that the R1 wave is generated by the interaction between the P1 and S1 waves based on our case study and the characteristic of Rayleigh waves (referring to the answer of Question 12).

14. Line 151. “The seismic measurements shown in Figure 3a are indeed a combination of both R1 and R2 waves.” These are not seismic measurements; they are synthetic data. It would perhaps be better to say “The surface waves shown in...”. Is the conclusion that Fig. 3a shows R1 and R2 waves based on the velocity match? It could be clearer what the authors are trying to convey with this sentence.

We have revised this accordingly in the manuscript: ‘The surface waves shown in Figure 3a are

indeed a combination of both R1 and R2 waves.’ In this sentence, our point is that the surface wave velocity captured in Figure 5a matches exactly the velocity of R1 and R2 modes calculated using the poro-mechanical dispersion solver. We found the velocity of R1 and R2 is 1,150 m/s and 450 m/s using the three-phase dispersion relation derived in this paper (Equation 1), which is exactly the same as what we captured in Figure 5a.

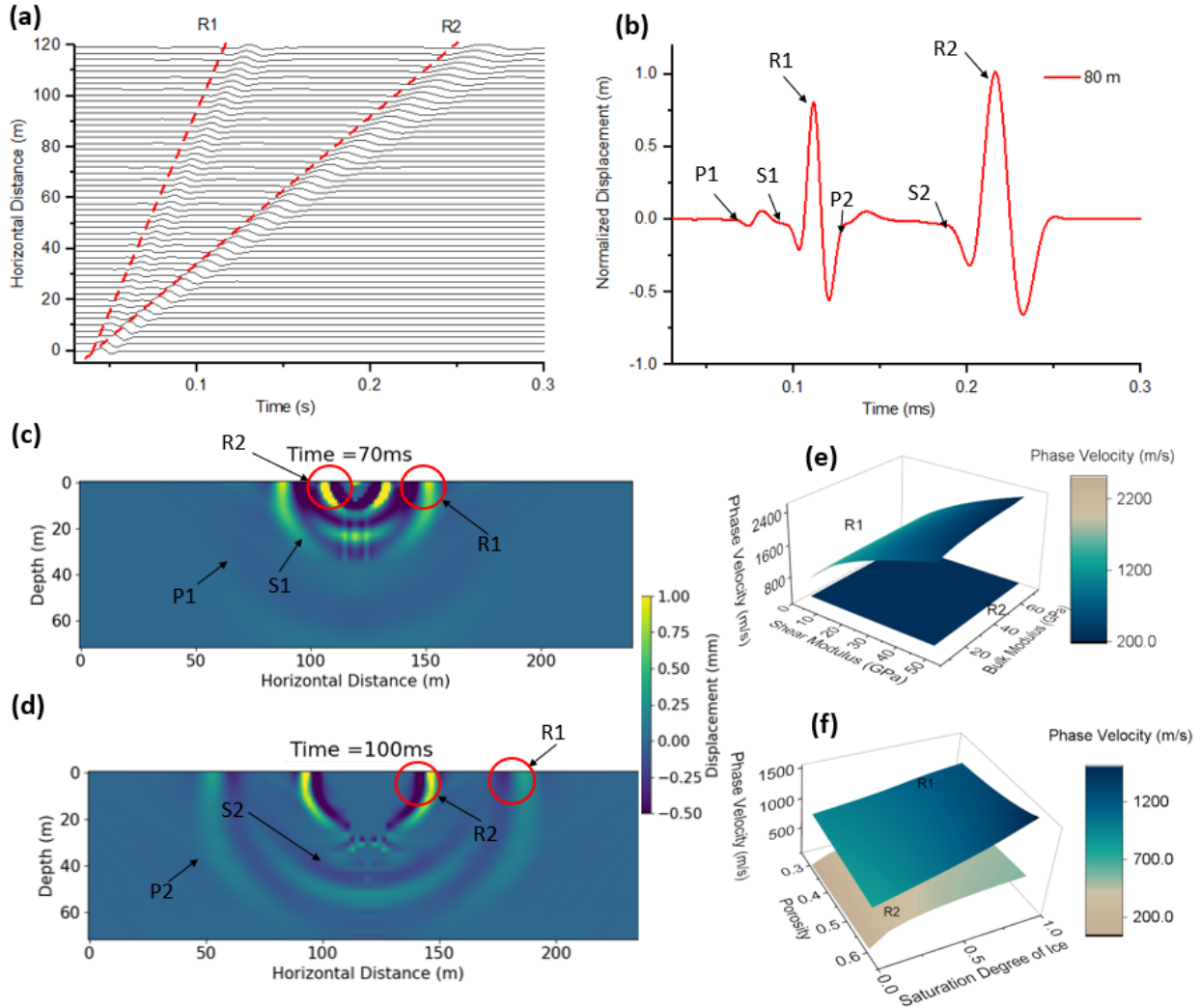


Figure 5: **(a)** Theoretical time-series measurements for R1 and R2 Rayleigh waves at the ground surface **(b)** Waveforms of R1, R2 and other wave modes at the offset of 80 m. **(c)** Displacement contour at time 70 ms. **(d)** Displacement contour at time 100 ms with the labeled R1 and R2 Rayleigh waves. **(e)** Effect of shear modulus and bulk modulus of the solid skeletal frame on phase velocity of R1 and R2 waves. **(f)** Effect of degree of saturation of ice on the phase velocity of R1 and R2 waves.

15. Figure 3. There is a lot of wasted space with zero amplitudes in Fig. 3a. While it shows the velocity moveout, it fails to illustrate the detailed waveforms of the R1 and R2 waves. It would be very useful to include at least one detailed timeseries example to illustrate the waveforms of these waves. The identification of the R1 and R2 waves is a key part of the main contribution of

this article and I do not think the current figure is adequate to illustrate their characteristics. There is also no colour scale on Fig. 3b-c.

We have added Figure 5b to illustrate the waveforms of R1 and R2 waves at the offset of 80 m. It is well known that the Rayleigh wave is generated by the combination of both P and S waves. More importantly, It is known that the Rayleigh wave is slightly slower than the shear wave velocity and the ratio of the Rayleigh wave and shear wave velocity ranges from 0.92-0.95 for the Poisson ratio greater than 0.3 (Kazemirad et al., 2013). Based on our case study in Section 3 in the manuscript, we can conclude that R1 waves appear due to the interaction of P1 and S1 waves since the phase velocity of R1 waves is slightly slower than the phase velocity of S1 waves. Similarly, R2 waves appear due to the interaction of P2 and S2 waves since the phase velocity of R2 waves is also slightly slower than the phase velocity of S2 waves. Therefore, the characteristics of Rayleigh waves that have been discovered in the literature also apply to the R1 and R2 wave modes. As shown in Figure 5b, the R1 and R2 wave have a much larger amplitude than any other components (e.g., P1, P2, S1 and S2), which is also consistent with the typical understanding of Rayleigh wave. Also the colour scale is added for the Figure 5c and 5d.

Reference:

Kazemirad, S., & Mongeau, L. (2013). Rayleigh wave propagation method for the characterization of a thin layer of biomaterials. *The Journal of the Acoustical Society of America*, 133(6), 4332-4342.

**16. Line 176.** How are the experimental dispersion spectra obtained? One assumes the phase shift method of Park (1999), but it is not stated. Are the dispersion curves manually picked or fitted to the spectral peak by a semi-automatic method? The only detail given is “The R1 and R2 Rayleigh waves are identified by visual inspection to obtain the experimental dispersion relations”. This seems radically insufficient given that the experimental dispersion relations are the key inversion constraint. One would expect that every detail surrounding the dispersion curve picking should be fully accounted for given their importance to the manuscript.

In the revised manuscript, the dispersion curve is automatically selected initially based on the highest intensity in the dispersion spectra using MASWave software (Olafsdottir et al., 2018). The uncertainties due to the selection of the dispersion curve from the dispersion spectra have been considered in the revised manuscript. Then a 90% confidence interval (labeled as lower bound, highest intensity and upper bound, as shown in Figure 3c and 3d) is considered to study the effect of the selection of dispersion curve on the inversion results.

Reference:

Olafsdottir, E. A., Erlingsson, S., & Bessason, B. (2018). Tool for analysis of multichannel analysis of surface waves (MASW) field data and evaluation of shear wave velocity profiles of soils. *Canadian Geotechnical Journal*, 55(2), 217-233.

**17. Line 185.** “The unfrozen ground is believed to have a degree of saturation of unfrozen water of about 100% (fully saturated)” is this based on previous studies? Please give a reference to support the assumption.

The direct sampling results reported by Szymański et al. (2013) confirmed that the study site is very wet and the water table is very high (around 15 cm). Figure 3b also shows the test site is extremely wet. Therefore, we can assume the degree of saturation of unfrozen water of about 100% (fully saturated).

Reference:

Szymański, W., Skiba, S., & Wojtuń, B. (2013). Distribution, genesis, and properties of Arctic soils: a case study from the Fuglebekken catchment, Spitsbergen. *Polish Polar Research*, 289-304.

**18.** Line 194: It does not seem clear that the soil type, its mineral composition or its organic carbon content have been resolved in the present study. It seems defensible that the presence of an ice rich layer has been demonstrated but the authors seem to be speculating far beyond this and these speculations should be either moderated or backed up with real or synthetic data examples to illustrate that they are feasible.

The shear modulus and bulk modulus in the proposed poro-mechanical approach are defined for the soil skeleton frame whose values are largely controlled by the mineral composition of the soil skeleton (Leclaire et al., 1994 and Carcione et al., 2001.).

Reference:

Carcione, J. M., & Seriani, G. (2001). Wave simulation in frozen porous media. *Journal of Computational Physics*, 170(2), 676-695.

Leclaire, P., Cohen-Ténoudji, F., & Aguirre-Puente, J. (1994). Extension of Biot's theory of wave propagation to frozen porous media. *The Journal of the Acoustical Society of America*, 96(6), 3753-3768.

**19.** Line 201: "Given the high ice-to-water ratio, we therefore interpret the permafrost is currently in a stable frozen state." The logic is unclear or not fully developed here. Unstable permafrost is distinguished by whether the ice and water saturation exceed the total pore volume of the ground in an unfrozen state. It seems that 22% water plus 91% ice (maximum values of uncertainty ranges) could exceed the pore volume in the permafrost layer and could therefore be considered unstable, though on the lower end 8.8% water plus 77% ice would be less than the pore volume in the frozen state of the permafrost. However, the frozen permafrost has elevated porosity compared to both the overlying and underlying layers. If we consider that water plus ice saturation in the permafrost is at least 86% of a frozen pore volume of 0.43-0.46, then it will likely be more than 100% saturation if the porosity in the unfrozen state is approximated by the porosity of the overlying active layer and underlying unfrozen ground (represented as 0.34-0.36 if we take the zone of overlap between the two porosity estimates). I think the authors should explicitly step through their assumptions and calculations in determining the stability of the permafrost, because this is a significant application area of their methodology and could be a major strength of the work if developed to its full potential.

Authors agree that unstable permafrost is distinguished by whether the ice and water saturation exceed the total pore volume of the ground in an unfrozen state. However, in our case it is almost impossible to accurately evaluate the total pore volume of permafrost in its unfrozen state since

we would have to conduct the seismic test when the permafrost thaws.

Here, we consider the segregated ice plays the same role as pore-ice from a continuum mechanics point of view. The growth of ice lenses is approximated as an increase in the soil porosity in a Representative Elementary Volume (REV) (the porosity is not the same as the unfrozen state since we have volumetric expansion in freezing process. Instead, as Michalowski et al. 2006 described, the porosity increases with the growth of ice lenses. Therefore, the total pore volume saturated with pore ice and unfrozen water is always the same as the porosity). Therefore, the determined volumetric ice content (Figure 2) can correspond to both pore-ice and segregated ice (ice lenses) as an average value. The degree of saturation of ice in permafrost can be roughly used to indicate whether permafrost is stable or not. In our revised inversion results, it is predicted that we have a low degree of saturation of unfrozen water (or a high degree of saturation of ice), as shown in Figure 2c. The relatively higher degree of saturation of unfrozen water at the offset distance from 120 m to 360 m can be due to the seawater infiltration. Due to freezing point depression contributed by the seawater infiltration (Wu et al. 2017), unfrozen water content at the offset distance from 120 m to 360 m is expected to be considerably higher than that at other offsets.

Reference:

Michalowski, R. L., & Zhu, M. (2006). Frost heave modelling using porosity rate function. *International journal for numerical and analytical methods in geomechanics*, 30(8), 703-722.

Wu, Y., Nakagawa, S., Kneafsey, T. J., Dafflon, B., & Hubbard, S. (2017). Electrical and seismic response of saline permafrost soil during freeze-thaw transition. *Journal of Applied Geophysics*, 146, 16-26.

**20.** Figure 4. The dispersion spectra use a colour scale that has an orange colour which appears in two different amplitude ranges making interpretation of the spectra ambiguous. I also don't understand why the manually picked dispersion curves are not overlain on the spectra. This is particularly important because the spectra are somewhat poorly resolved and identification of the precise dispersion relation is far from straightforward from these data.

In the revised manuscript, the dispersion curve is automatically selected initially based on the highest intensity in the dispersion spectra using MASWave software (Olafsdottir et al., 2018). The uncertainties due to the selection of the dispersion curve from the dispersion spectra have been considered in the revised manuscript. Then a 90% confidence interval, as shown in Figure 3c and 3d, is considered to study the effect of the selection of dispersion curve on the inversion results.

Reference:

Olafsdottir, E. A., Erlingsson, S., & Bessason, B. (2018). Tool for analysis of multichannel analysis of surface waves (MASW) field data and evaluation of shear wave velocity profiles of soils. *Canadian Geotechnical Journal*, 55(2), 217-233.

**21.** Figure 5. It is concerning that the prediction envelope of the R2 dispersion relation is concave down at frequencies below 20 Hz, while the experimental measurement is concave up. Looking at the experimental dispersion image for the R2 wave in Fig. 4d it seems quite clear that low frequencies should trend towards high phase velocities. The implication here is that some important

parameter of the system is not resolved by the inversion. I will come back to this, but it may be the root cause of the anomalous result reported for the 360-480m section.

In our previous inversion analysis, we assumed that the last layer in our model is the unfrozen ground which may be unrealistic considering that the penetrating depth is roughly half of the maximum wavelength (Olafsdottir et al., 2018). For instance, the maximum wavelength in Section 1 is about 22 m (calculated using a phase velocity of 404 m/s at the frequency of 18 Hz). The maximum wavelength for Section 2 to 5 can be calculated in a similar manner. The average maximum wavelength for the entire investigation areas is around 21 m. Therefore, the penetrating depth in the MASW survey presented in this study is only about 11 m. It was reported that the permafrost layer in the studied site can go up to 100 m (Dolnicki et al., 2013; Glazer et al., 2018). Therefore, in the revised paper, we considered the last layer to have a degree of saturation of unfrozen water ranging from 1% to 99%. In this way, the last layer can be either permafrost or unfrozen ground. We have also applied the automatic methods for the selection of dispersion curves (instead of relying on visual inspection that we used in the original draft) using MASWave software (Olafsdottir, 2018). The misfits (RMS) between the R1 experimental and numerical dispersion curves at Section 4 have been significantly reduced from 49.6 to only 4.7, as shown in Figure 1g.

Reference:

Glazer, M., Dobiński, W., Marciniak, A., Majdański, M., & Błaszczuk, M. (2020). Spatial distribution and controls of permafrost development in non-glacial Arctic catchment over the Holocene, Fuglebekken, SW Spitsbergen. *Geomorphology*, 358, 107128.

Dolnicki, P., Grabiec, M., Puczko, D., Gawor, L., Budzik, T., & Klementowski, J. (2013). Variability of temperature and thickness of permafrost active layer at coastal sites of Svalbard.

**22.** Line 225. “the permafrost table is generally located at about 4 m below the ground surface, except at the offset distance from 360 m to 480 m where the permafrost table is located at 1.1m below the ground surface.” Is there a geologic or geomorphologic explanation for this variation, e.g., topography, vegetation, surface-water etc.? Is there otherwise some other geophysical dataset that could corroborate this? It seems rather implausible that the permafrost table is so dramatically elevated at one anomalous location. If the anomalous result at 360-480 m cannot be explained from a reasonable physical or geological perspective then it rather points towards a significant degree of uncertainty or instability in the inversion.

In the revised manuscript, the comparison of the inversion results using the proposed hybrid inverse and multi-phase poro-mechanical approach and inversion results from ERT survey provided by Glazer et al., (2020) has been added. It was reported by Glazer et al., (2020) that the permafrost table is located at a depth of about 2 m for a span of 20 m. The new inversion results in terms of the thickness of the active layer were also validated using the results reported by Dobiński et al., (2010) and Dolnicki et al., (2013) by the direct probing method. It was also reported by Dobiński et al., (2010) and Dolnicki et al., (2013) that the active layer in Svalbard is approximately 1.65–2.5 m deep. The direct sampling results reported by Szymański et al. (2013) confirmed that the study site is very wet and the water table is very high (around 15 cm). It was reported by Szymański et al. (2013) that this study site also contains a lot of coarse sandy soils, gravels as well as around 20% silty clay based on the direct sampling methods at the top 15 cm. Our inversion results, as shown

in Figure 2, predicted that the permafrost table is generally located at about 1.5-1.9 m below the ground surface, which is consistent with the ERT results reported by Glazer et al., (2020) and results reported by Dobiński et al., (2010) and Dolnicki et al., (2013) using the direct probing method.

In our previous inversion analysis, we assumed that the last layer in our model is the unfrozen ground which may be unrealistic considering that the penetrating depth is roughly half of the maximum wavelength (Olafsdottir et al., 2018). For instance, the maximum wavelength in Section 1 is about 22 m (calculated using a phase velocity of 404 m/s at the frequency of 18 Hz). The maximum wavelength for Section 2 to 5 can be calculated in a similar manner. The average maximum wavelength for the entire investigation areas is around 21 m. Therefore, the penetrating depth in the MASW survey presented in this study is only about 11 m. It was reported that the permafrost layer in the studied site can go up to 100 m (Dolnicki et al., 2013; Glazer et al., 2018). Therefore, in the revised paper, we considered the last layer to have a degree of saturation of unfrozen water ranging from 1% to 99%. In this way, the last layer can be either permafrost or unfrozen ground. We have also applied the automatic methods for the selection of dispersion curves (instead of relying on visual inspection that we used in the original draft) using MASWave software (Olafsdottir, 2018). The misfits (RMS) between the R1 experimental and numerical dispersion curves at Section 4 have been significantly reduced from 49.6 to only 4.7, as shown in Figure 1g.

Based on the field description of the testing site by Glazer et al., (2020), the unconsolidated sedimentary rock contains a high proportion of pore spaces; consequently, they can accumulate a large volume of pore-water or pore-ice. Our inversion results showed that the porosity of the active layer ranges from 0.56 to 0.69, which is consistent with the field description by Glazer et al., (2020). The unfrozen water content in the second permafrost layer was predicted ranging from 0.05-0.17. Li et al. (2020) and Zhang et al. (2020) showed that the residual volumetric unfrozen water content for silty-clay, clay, medium sand, and fine sand is 0.12, 0.08, 0.06 and 0.03, respectively. Our inversion results predicted that soils are mostly silty-clay or clay (Section 1-3) and sandy soils, which are also consistent with the results described by Szymański et al. (2013). Figure 2e shows the variation of the shear modulus of soil skeleton predicted by the proposed hybrid inverse and multi-phase poro-mechanical approach. The predicted shear modulus in the first layer at the offset distance of 0 to 360 m ranges from 4 GPa to 7.9 GPa, which represents clay soils (Helgerud ET AL. 1999). At the offset distance of 360 to 600 m, the estimated shear modulus in the first layer ranges from 27 GPa to 33 GPa, which corresponds to soils with calcite constituents (Helgerud et al. 1999). Calcite most commonly occurs in sedimentary rock or gravels (Schmid et al., 1987), which is consistent with the field description given by Glazer et al. 2020 and Szymański et al. (2013).

Reference:

Glazer, M., Dobiński, W., Marciniak, A., Majdański, M., & Błaszczuk, M. (2020). Spatial distribution and controls of permafrost development in non-glacial Arctic catchment over the Holocene, Fuglebekken, SW Spitsbergen. *Geomorphology*, 358, 107128.

Szymański, W., Skiba, S., & Wojtuń, B. (2013). Distribution, genesis, and properties of Arctic soils: a case study from the Fuglebekken catchment, Spitsbergen. *Polish Polar Research*, 289-304.

Helgerud, M. B., Dvorkin, J., Nur, A., Sakai, A., & Collett, T. (1999). Elastic-wave velocity in marine sediments with gas hydrates: Effective medium modeling. *Geophysical Research Letters*, 26(13),

2021-2024.

Li, Z., Chen, J., & Sugimoto, M. (2020). Pulsed NMR measurements of unfrozen water content in partially frozen soil. *Journal of Cold Regions Engineering*, 34(3), 04020013.

Zhang, M., Zhang, X., Lai, Y., Lu, J., & Wang, C. (2020). Variations of the temperatures and volumetric unfrozen water contents of fine-grained soils during a freezing–thawing process. *Acta Geotechnica*, 15(3), 595-601.

Dolnicki, P., Grabiec, M., Puczko, D., Gawor, L., Budzik, T., & Klementowski, J. (2013). Variability of temperature and thickness of permafrost active layer at coastal sites of Svalbard.

Dobiński, W., & Leszkiewicz, J. (2010). Active layer and permafrost occurrence in the vicinity of the Polish Polar Station, Hornsund, Spitsbergen in the light of geophysical research. *Problemy Klimatologii Polarnej*, 20, 129-142.

**23.** Line 233. “Sufficient agreement exists between the numerical and experimental dispersion relations for the R2 wave (Figure 7d) which confirms the acceptance of the predicted values for the volumetric ice content (calculated as the product of porosity and the degree of saturation of ice) and porosity”. I find it difficult to agree with this statement. The model and experimental dispersion curves have notably poorer correspondence for the 360-480 m section, which is the only section that gives a significantly different inversion result. This points towards model misfit rather than physical reality.

In our previous inversion analysis, we assumed that the last layer in our model is the unfrozen ground which may be unrealistic considering that the penetrating depth is roughly half of the maximum wavelength (Olafsdottir et al., 2018). For instance, the maximum wavelength in Section 1 is about 22 m (calculated using a phase velocity of 404 m/s at the frequency of 18 Hz). The maximum wavelength for Section 2 to 5 can be calculated in a similar manner. The average maximum wavelength for the entire investigation areas is around 21 m. Therefore, the penetrating depth in the MASW survey presented in this study is only about 11 m. It was reported that the permafrost layer in the studied site can go up to 100 m (Dolnicki et al., 2013; Glazer et al., 2018). Therefore, in the revised paper, we considered the last layer to have a degree of saturation of unfrozen water ranging from 1% to 99%. In this way, the last layer can be either permafrost or unfrozen ground. We have also applied the automatic methods for the selection of dispersion curves (instead of relying on visual inspection that we used in the original draft) using MASWave software (Olafsdottir, 2018). The misfits (RMS) between the R1 experimental and numerical dispersion curves at Section 4 have been significantly reduced from 49.6 to only 4.7, as shown in Figure 1g.

**24.** Figure 7. It is not convincing that the anomalously shallow permafrost table, high ice content result at 360-480 m reflects a real variation in ground structure/properties. The experimental dispersion curves look quite similar in the overlapping frequency ranges, but the 360-480 m dispersion curve extends to lower frequencies than the others do. It would be beneficial to examine a figure plotting all dispersion curves on a shared axis so the reader can see where and by how much they really vary (but this is of course up to the authors discretion). In all cases, it looks like the experimental dispersion curves are concave up at low frequencies and the R2 prediction envelopes are concave down. This mismatch is exacerbated for the 360-480 m section, which extends

to lower frequencies than the others and therefore leads to the anomalous result. It is difficult to say which result is closer to reality because of a lack of comparison with ground truth observations or other geophysical data sets. The frequency range from 13-20 Hz is where the phase velocity of the R2 wave varies most significantly (Fig 4d) so it is concerning that the inversion seems to have problems matching the experimental curve in exactly this part of the frequency spectrum.

We have plotted all dispersion curves on a shared axis to show where and by how much these dispersion curves vary. In our previous inversion analysis, we assumed that the last layer in our model is the unfrozen ground which may be unrealistic considering that the penetrating depth is roughly half of the maximum wavelength (Olafsdottir et al., 2018). For instance, the maximum wavelength in Section 1 is about 22 m (calculated using a phase velocity of 404 m/s at the frequency of 18 Hz). The maximum wavelength for Section 2 to 5 can be calculated in a similar manner. The average maximum wavelength for the entire investigation areas is around 21 m. Therefore, the penetrating depth in the MASW survey presented in this study is only about 11 m. It was reported that the permafrost layer in the studied site can go up to 100 m (Dolnicki et al., 2013; Glazer et al., 2018). Therefore, in the revised paper, we considered the last layer to have a degree of saturation of unfrozen water ranging from 1% to 99%. In this way, the last layer can be either permafrost or unfrozen ground. We have also applied the automatic methods for the selection of dispersion curves (instead of relying on visual inspection that we used in the original draft) using MASWave software (Olafsdottir, 2018). The misfits (RMS) between the R1 experimental and numerical dispersion curves at Section 4 have been significantly reduced from 49.6 to only 4.7, as shown in Figure 1g.

More importantly, we have validated our results with the ERT investigation, direct probing and testing pit investigation reported by Glazer et al. 2020, Szymański et al. 2013, Dobiński et al., (2010) and Dolnicki et al., (2013). The new inversion results in terms of the thickness of the active layer were also validated using the results reported by Dobiński et al., (2010) and Dolnicki et al., (2013) by the direct probing method. It was also reported by Dobiński et al., (2010) and Dolnicki et al., (2013) that the active layer in Svalbard is approximately 1.65–2.5 m deep. The direct sampling results reported by Szymański et al. (2013) confirmed that the study site is very wet and the water table is very high (around 15 cm). It was reported by Szymański et al. (2013) that this study site also contains a lot of coarse sandy soils, gravels as well as around 20% silty clay based on the direct sampling methods at the top 15 cm. Our inversion results, as shown in Figure 2, predicted that the permafrost table is generally located at about 1.5-1.9 m below the ground surface, which is consistent with the ERT results reported by Glazer et al., (2020) and results reported by Dobiński et al., (2010) and Dolnicki et al., (2013) using the direct probing method.

Based on the field description of the testing site by Glazer et al., (2020), the unconsolidated sedimentary rock contains a high proportion of pore spaces; consequently, they can accumulate a large volume of pore-water or pore-ice. Our inversion results showed that the porosity of the active layer ranges from 0.56 to 0.69, which is consistent with the field description by Glazer et al., (2020). The unfrozen water content in the second permafrost layer was predicted ranging from 0.05-0.17. Li et al. (2020) and Zhang et al. (2020) showed that the residual volumetric unfrozen water content for silty-clay, clay, medium sand, and fine sand is 0.12, 0.08, 0.06 and 0.03, respectively. Our inversion results predicted that soils are mostly silty-clay or clay (Section 1-3) and sandy soils, which are also consistent with the results described by Szymański et al. (2013). Figure 2e shows the variation of the shear modulus of soil skeleton predicted by the proposed hybrid inverse and multi-phase poro-mechanical approach. The predicted shear modulus in the first layer at the off-

set distance of 0 to 360 m ranges from 4 GPa to 7.9 GPa, which represents clay soils (Helgerud ET AL. 1999). At the offset distance of 360 to 600 m, the estimated shear modulus in the first layer ranges from 27 GPa to 33 GPa, which corresponds to soils with calcite constituents (Helgerud et al. 1999). Calcite most commonly occurs in sedimentary rock or gravels (Schmid et al., 1987), which is consistent with the field description given by Glazer et al. 2020 and Szymański et al. (2013).

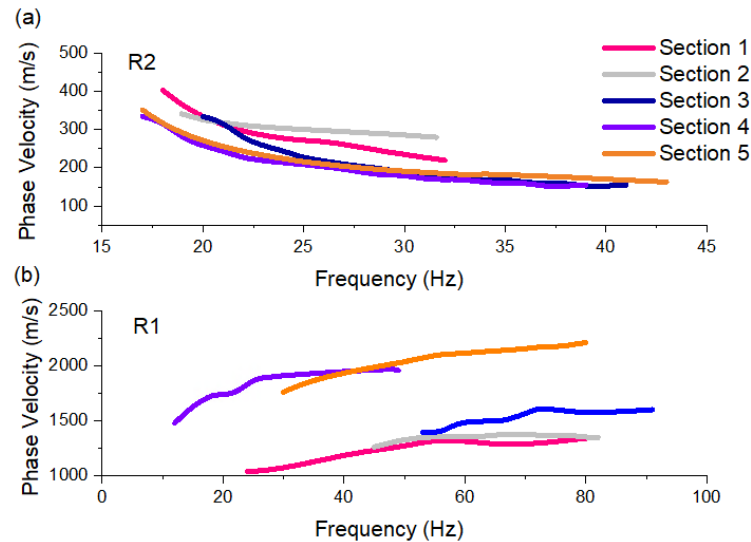


Figure 6: Summary of dispersion measurements. **(a)** Dispersion curves of R2 mode. **(b)** Dispersion curves of R1 mode.

Reference:

Li, Z., Chen, J., & Sugimoto, M. (2020). Pulsed NMR measurements of unfrozen water content in partially frozen soil. *Journal of Cold Regions Engineering*, 34(3), 04020013.

Zhang, M., Zhang, X., Lai, Y., Lu, J., & Wang, C. (2020). Variations of the temperatures and volumetric unfrozen water contents of fine-grained soils during a freezing–thawing process. *Acta Geotechnica*, 15(3), 595-601.

Szymański, W., Skiba, S., & Wojtuń, B. (2013). Distribution, genesis, and properties of Arctic soils: a case study from the Fuglebekken catchment, Spitsbergen. *Polish Polar Research*, 289-304.

Helgerud, M. B., Dvorkin, J., Nur, A., Sakai, A., & Collett, T. (1999). Elastic-wave velocity in marine sediments with gas hydrates: Effective medium modeling. *Geophysical Research Letters*, 26(13), 2021-2024.

Carcione, J. M., & Seriani, G. (2001). Wave simulation in frozen porous media. *Journal of Computational Physics*, 170(2), 676-695.

Glazer, M., Dobiński, W., Marciniak, A., Majdański, M., & Błaszczuk, M. (2020). Spatial distribution and controls of permafrost development in non-glacial Arctic catchment over the Holocene, Fuglebekken, SW Spitsbergen. *Geomorphology*, 358, 107128.

25. Line 238. “at the offset distance from 360 m to 480 m the coldest temperature of about -12 C (Figure 7e) occurs in the permafrost layer, which is highly related to the high ice content in this section.” Again, a more nuanced interpretation is required. It is difficult to accept that the anomalous data section, with the poorest correspondence between model and experimental dispersion curves can simply be interpreted as a real physical effect without giving a supporting physical explanation.

Based on our new inversion results, the degree saturation of unfrozen water and porosity is 14% and 0.7, respectively at the offset distance from 360 m to 480 m. The volumetric unfrozen water content (calculated as the product of porosity and the degree of saturation of unfrozen water) in the permafrost layer is about 0.10. Li et al. (2020) and Zhang et al. (2020) showed that the residual volumetric unfrozen water content for silty-clay, clay, medium sand, and fine sand is 0.12, 0.08, 0.06 and 0.03, respectively. These predictions fit well within the reasonable range of volumetric unfrozen water content for clay or clayey silt. Sufficient agreement exists between the numerical and experimental dispersion relations for the R2 wave (Figure 1f) which confirms the acceptance of the predicted values for the volumetric ice content (calculated as the product of porosity and the degree of saturation of ice) and porosity. Meanwhile, based on the mechanical properties of the solid skeletal frame (most likely clayey or clayey silt soil), we can reasonably consider the permafrost layer at the offset distance from 360 m to 480 m to be ice-rich and ice segregation layers are expected to contribute to its relatively higher volumetric ice content. Here, we consider the segregated ice plays the same role as pore-ice from a continuum mechanics point of view. The growth of ice lenses is approximated as an increase in the soil porosity (the porosity is not the same as the unfrozen state since we have volumetric expansion in the freezing process). Therefore, the determined volumetric ice content (Figure 2) can correspond to both pore-ice and segregated ice (ice lenses) as an average value. In our revised inversion results, it is predicted that we have low degree of saturation of unfrozen water (or high degree of saturation of ice) , as shown in Figure 2c. The relatively higher degree of saturation of unfrozen water at the offset distance from 120 m to 360 m can be due to the seawater infiltration. Due to freezing point depression contributed by the seawater infiltration (Wu et al. 2017), unfrozen water content at the offset distance from 120 m to 360 m is expected to be considerably higher than that at other offsets.

In terms of the estimated temperature distribution, our new inversion results predicted that at the offset distance from 480 m to 600 m the coldest temperature of about -14 °C (Figure 7) occurs in the permafrost layer, which is highly related to the high ice content in this section.

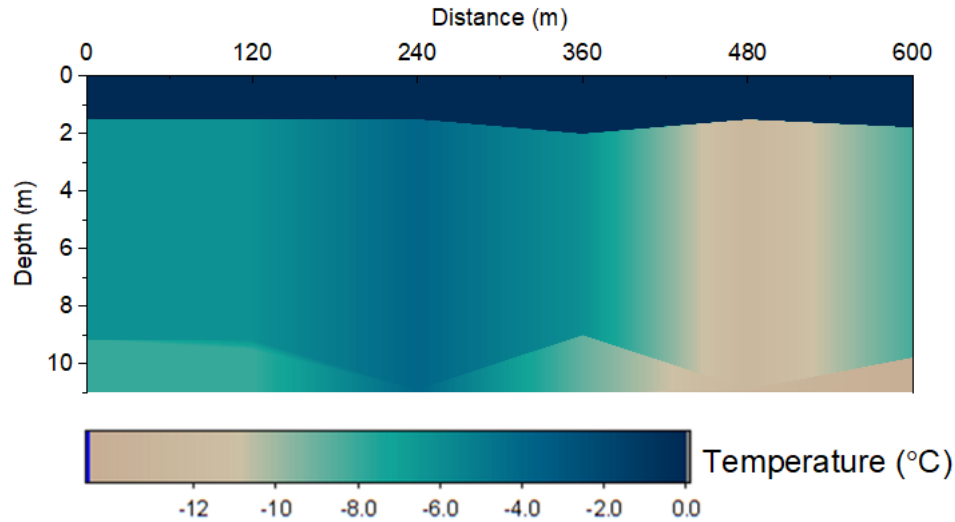


Figure 7: Inversion results in terms of soil temperature at the offset distance from 0 m to 600 m.

Reference:

Michalowski, R. L., & Zhu, M. (2006). Frost heave modelling using porosity rate function. *International journal for numerical and analytical methods in geomechanics*, 30(8), 703-722.

Wu, Y., Nakagawa, S., Kneafsey, T. J., Dafflon, B., & Hubbard, S. (2017). Electrical and seismic response of saline permafrost soil during freeze-thaw transition. *Journal of Applied Geophysics*, 146, 16-26.

Li, Z., Chen, J., & Sugimoto, M. (2020). Pulsed NMR measurements of unfrozen water content in partially frozen soil. *Journal of Cold Regions Engineering*, 34(3), 04020013.

Zhang, M., Zhang, X., Lai, Y., Lu, J., & Wang, C. (2020). Variations of the temperatures and volumetric unfrozen water contents of fine-grained soils during a freezing–thawing process. *Acta Geotechnica*, 15(3), 595-601.

Szymański, W., Skiba, S., & Wojtuń, B. (2013). Distribution, genesis, and properties of Arctic soils: a case study from the Fuglebekken catchment, Spitsbergen. *Polish Polar Research*, 289-304.

**26.** Line 253. “the mechanical properties of the solid skeletal frame can reveal the type of soil”. How much overlap in mechanical properties is there for different types of soils and how does the estimation compare with the soil pit sampling study of, e.g., Szymański et al. (2013) which covers the Fuglebekken area?

The mechanical properties (especially for the shear modulus) of the solid skeletal frame for soils containing clay minerals, calcite, quartz are very different (around 6.85 GPa, 32 GPa and 45 GPa, respectively) (Helgerud et al. 1999; Vanorio et al. 2003). These minerals can significantly alter the elastic behavior of soils or rocks (Vanorio et al. 2003). We expect to have overlaps in the mechanical properties when the soils or rocks contain various mineral components. However, the mechanical properties of the solid skeletal frame are still capable of indicating the majority of the

mineral components in soils or rocks.

It was reported by Szymański et al. (2013) that this study site also contains a lot of coarse sandy soils, gravels as well as around 20% silty clay based on the direct sampling methods at the top 15 cm. Figure 2e shows the variation of the shear modulus of soil skeleton predicted by the proposed hybrid inverse and multi-phase poro-mechanical approach. The predicted shear modulus in the first layer at the offset distance of 0 to 360 m ranges from 4 GPa to 7.9 GPa, which represents clay soils (Helgerud et al. 1999). At the offset distance of 360 to 600 m, the estimated shear modulus in the first layer ranges from 27 GPa to 33 GPa, which corresponds to soils with calcite constituents (Helgerud et al. 1999). Calcite most commonly occurs in sedimentary rock or gravels (Schmid et al., 1987), which is consistent with the field description given by Glazer et al. 2020 and Szymański et al. (2013).

Reference:

Schmid, S. M., Panozzo, R., & Bauer, S. (1987). Simple shear experiments on calcite rocks: rheology and microfabric. *Journal of structural Geology*, 9(5-6), 747-778.

Szymański, W., Skiba, S., & Wojtuń, B. (2013). Distribution, genesis, and properties of Arctic soils: a case study from the Fuglebekken catchment, Spitsbergen. *Polish Polar Research*, 289-304.

Glazer, M., Dobiński, W., Marciniak, A., Majdański, M., & Błaszczuk, M. (2020). Spatial distribution and controls of permafrost development in non-glacial Arctic catchment over the Holocene, Fuglebekken, SW Spitsbergen. *Geomorphology*, 358, 107128.

Helgerud, M. B., Dvorkin, J., Nur, A., Sakai, A., & Collett, T. (1999). Elastic-wave velocity in marine sediments with gas hydrates: Effective medium modeling. *Geophysical Research Letters*, 26(13), 2021-2024.

Vanorio, T., Prasad, M., & Nur, A. (2003). Elastic properties of dry clay mineral aggregates, suspensions and sandstones. *Geophysical Journal International*, 155(1), 319-326.

**27. Line 256.** “if the mechanical properties of the solid skeletal frame correspond to the ones for peat we can perform more detailed investigation to assess the sensitivity of the permafrost to greenhouse gases emission.” It is important to communicate that this application remains hypothetical, since the ability to resolve the presence of a peat layer has not been demonstrated in this study. Perhaps the authors would consider adding a synthetic data example including a peat layer if they feel this is an important application to emphasize.

We have clarified that the detection of the peat permafrost layer and the corresponding greenhouse gases emission will be our future study. This application still requires in-depth investigation and research. A detailed description for this application was given in the answer to Question 4 and 10.

**28. Line 260.** “we can reasonably consider the permafrost layer at the offset distance from 360 m to 480 m to be ice-rich and ice segregation layers are expected to contribute to its relatively higher volumetric ice content.” This seems to require an assumption of the porosity in the unfrozen state, which is not given explicitly but should be, so that the reader can follow the authors line of reasoning. It would also be valuable to discuss if it is physically reasonable for a change to occur at

this location alone, while all other locations consistently gave a different result.

Based on our new inversion results, the degree saturation of unfrozen water and porosity is 14% and 0.7, respectively at the offset distance from 360 m to 480 m. The volumetric unfrozen water content (calculated as the product of porosity and the degree of saturation of unfrozen water) in the permafrost layer is about 0.10. Li et al. (2020) and Zhang et al. (2020) showed that the residual volumetric unfrozen water content for silty-clay, clay, medium sand, and fine sand is 0.12, 0.08, 0.06 and 0.03, respectively. These predictions fit well within the reasonable range of volumetric unfrozen water content for clay or clayey silt. Sufficient agreement exists between the numerical and experimental dispersion relations for the R2 wave (Figure 1f) which confirms the acceptance of the predicted values for the volumetric ice content (calculated as the product of porosity and the degree of saturation of ice) and porosity. Meanwhile, based on the mechanical properties of the solid skeletal frame (most likely clayey or clayey silt soil), we can reasonably consider the permafrost layer at the offset distance from 360 m to 480 m to be ice-rich and ice segregation layers are expected to contribute to its relatively higher volumetric ice content. Here, we consider the segregated ice plays the same role as pore-ice from a continuum mechanics point of view. The growth of ice lenses is approximated as an increase in the soil porosity (the porosity is not the same as the unfrozen state since we have volumetric expansion and ice segregation in the freezing process). Therefore, the determined volumetric ice content (Figure 2) can correspond to both pore-ice and segregated ice (ice lenses) as an average value. In our revised inversion results, it is predicted that we have a low degree of saturation of unfrozen water (or high degree of saturation of ice), as shown in Figure 2c. The relatively higher degree of saturation of unfrozen water at the offset distance from 120 m to 360 m can be due to the seawater infiltration. Due to freezing point depression contributed by the seawater infiltration (Wu et al. 2017), unfrozen water content at the offset distance from 120 m to 360 m is expected to be considerably higher than that at other offsets.

Reference:

Michalowski, R. L., & Zhu, M. (2006). Frost heave modelling using porosity rate function. *International journal for numerical and analytical methods in geomechanics*, 30(8), 703-722.

Wu, Y., Nakagawa, S., Kneafsey, T. J., Dafflon, B., & Hubbard, S. (2017). Electrical and seismic response of saline permafrost soil during freeze-thaw transition. *Journal of Applied Geophysics*, 146, 16-26.

Li, Z., Chen, J., & Sugimoto, M. (2020). Pulsed NMR measurements of unfrozen water content in partially frozen soil. *Journal of Cold Regions Engineering*, 34(3), 04020013.

Zhang, M., Zhang, X., Lai, Y., Lu, J., & Wang, C. (2020). Variations of the temperatures and volumetric unfrozen water contents of fine-grained soils during a freezing–thawing process. *Acta Geotechnica*, 15(3), 595-601.

Szymański, W., Skiba, S., & Wojtuń, B. (2013). Distribution, genesis, and properties of Arctic soils: a case study from the Fuglebekken catchment, Spitsbergen. *Polish Polar Research*, 289-304.

29. Line 267. “The uncertainty originates from the non-uniqueness in the inverse analysis (local minima problem) and the limited number of constraints in the inversion analysis”. The sensitivity to small changes in the experimental dispersion curves is not adequately covered in the

manuscript. For example, the 360-480 m section has an experimental dispersion curve that appears quite similar to the other sections, but extends to a lower frequency range and gives a substantially different inversion result. More generally, there is always some uncertainty in picking the dispersion curve from experimental data and it is unclear how this uncertainty may propagate through the inversion. How do the results differ for a set of dispersion curves that are indistinguishably close from an experimental perspective? The R1 dispersion spectra in particular is quite poorly resolved (Fig. 4c) so one must assume some degree of uncertainty is associated with the picked dispersion curve.

We have selected lower and upper bounds of dispersion spectra to study the uncertainty that propagates through the inversion analysis. The dispersion curve is automatically selected initially based on the highest intensity in the dispersion spectra using MASWave software (Olafsdottir et al., 2018). The uncertainties due to the selection of the dispersion curve from the dispersion spectra have been considered in the revised manuscript. Then a 90% confidence interval, as shown in Figure 3f and 3g, is considered to study the effect of the selection of dispersion curve on the inversion results.

Figure 8a shows the probabilistic distribution of the degree of saturation of unfrozen water with depth in Section 1. Our results show that the active layer has a thickness of about 1.5 m. The predicted permafrost layer (second layer) has a nearly 32% of degree of saturation of unfrozen pore water. Figure 8b shows the degree of saturation of ice with depth. The degree of saturation of ice in the permafrost layer (second layer) ranges from 67% to 79%. Figure 8c illustrates the porosity distribution with depth. The porosity is around 0.60 in the first layer (active layer), from 0.40 to 0.47 in the second layer (permafrost) and from 0.56 to 0.59 in the third layer. Figure 8d and 8e show the predicted mechanical properties of the solid skeletal frame (shear modulus and bulk modulus) in each layer. It was reported by Szymański et al. (2013) that this study site also contains a lot of coarse sandy soils, gravels as well as around 20% silty clay based on the direct sampling methods at the top 15 cm. The predicted shear modulus and bulk modulus for the solid skeletal frame in the permafrost layer (second layer) are about 13 GPa and 12.7 GPa, which are in the range for silty-clayey soils (Vanorio et al. 2003) and are also consistent with the local soil types described by Szymański et al. (2013). The predicted shear modulus and bulk modulus for the solid skeletal frame in the third layer are about 4 GPa and 10 GPa, which are in the range for clayey soils (Vanorio et al. 2003). Figure 8f and 8g show the comparison between the numerical and experimental dispersion relations for R2 and R1 waves, respectively. The numerical predictions show good agreement with the experimental dispersion curves for both R1 and R2 waves. The uncertainty analyses for other Sections are performed in a similar manner.

Reference:

Olafsdottir, E. A., Erlingsson, S., & Bessason, B. (2018). Tool for analysis of multichannel analysis of surface waves (MASW) field data and evaluation of shear wave velocity profiles of soils. *Canadian Geotechnical Journal*, 55(2), 217-233.

Vanorio, T., Prasad, M., & Nur, A. (2003). Elastic properties of dry clay mineral aggregates, suspensions and sandstones. *Geophysical Journal International*, 155(1), 319-326.

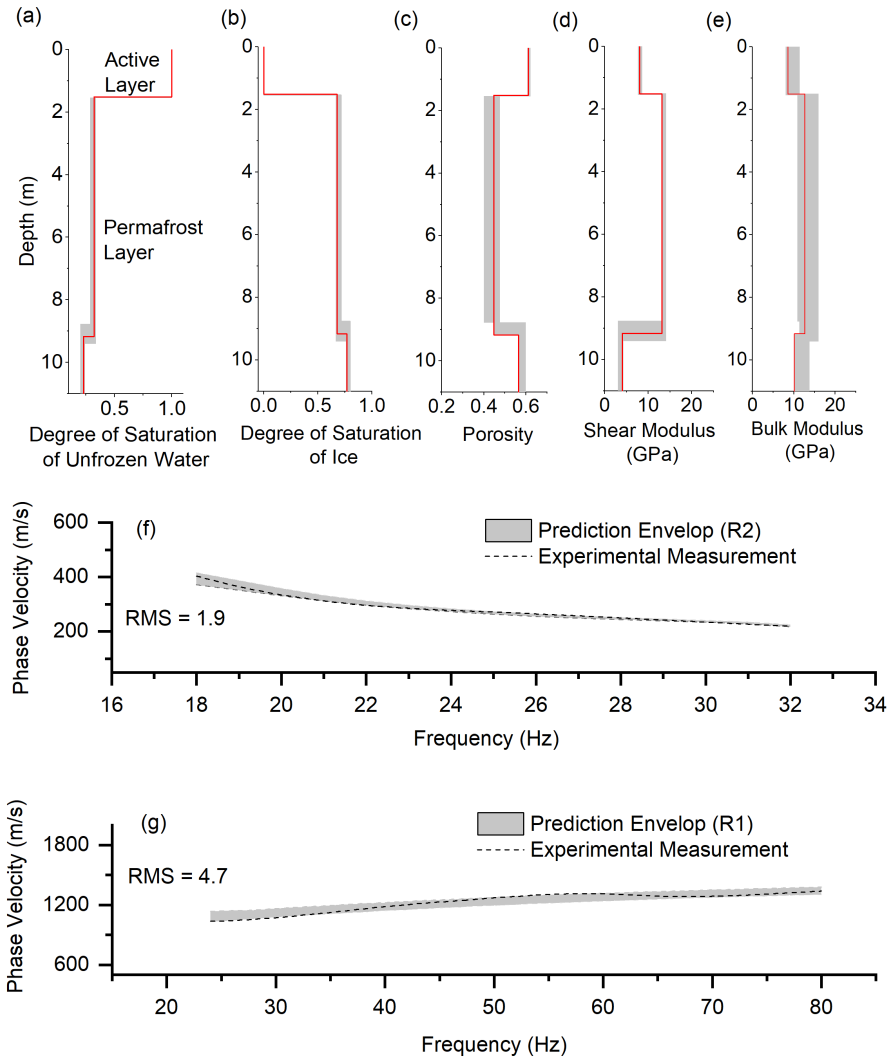


Figure 8: Surface wave inversion results for Section 1: 0m to 120m. **(a)** Degree of saturation of unfrozen water, **(b)** Degree of saturation of ice, **(c)** Porosity distribution, **(d)** Shear modulus of solid skeletal frame, **(e)** Bulk modulus of solid skeletal frame, **(f)** Experimental and numerical dispersion curves for R2 wave, **(g)** Experimental and numerical dispersion curves for R1 wave.

30. Line 268. “recommended to use other geophysical methods to improve the resolution and reduce uncertainty of the permafrost mapping.” Why are the inversion results of the field example not discussed in the context of existing geophysical and direct sampling results? This is a crucial step in qualifying the validity of the proposed methodology.

In the revised manuscript, we have added the comparison of the inversion results from the proposed approach and results from the ERT survey from Glazer et al., (2020) as well as the site description reported by Dobiński et al., (2010) and Dolnicki et al., (2013). A detailed description in the context of existing geophysical (ERT) and direct sampling results was given in the answer to Question 22.

Reference:

Glazer, M., Dobiński, W., Marciniak, A., Majdański, M., & Błaszczuk, M. (2020). Spatial distribution and controls of permafrost development in non-glacial Arctic catchment over the Holocene, Fuglebekken, SW Spitsbergen. *Geomorphology*, 358, 107128.

Dolnicki, P., Grabiec, M., Puczko, D., Gawor, L., Budzik, T., & Klementowski, J. (2013). Variability of temperature and thickness of permafrost active layer at coastal sites of Svalbard.

Dobiński, W., & Leszkiewicz, J. (2010). Active layer and permafrost occurrence in the vicinity of the Polish Polar Station, Hornsund, Spitsbergen in the light of geophysical research. *Problemy Klimatologii Polarnej*, 20, 129-142.

**31. Line 272.** “The proposed hybrid inverse and multi-phase poro-mechanical approach can potentially be used for the design of an early warning system for permafrost by means of an active or passive seismic test.” It seems that too much emphasis is placed on this hypothetical future application while the more important topic of qualifying the inversion results in the context of other geophysical methods, direct sampling, geological and geomorphological understanding etc. is lacking. There is no convincing argument that changes in poro-mechanical properties that would be detectable with the current methodology occur in advance of physical surface expressions such as subsidence or cracks in structures. This would presumably be a key requirement of an early warning system.

We have clarified the application of early detection and warning systems to detect the presence of layers vulnerable to permafrost carbon feedback and emission of greenhouse gases into the atmosphere will be the goal of future study, as discussed in detail in the response to Question 4. Also, we have added the comparison of the inversion results from the proposed approach and results from the ERT survey from Glazer et al., (2020) as well as the site description reported by Dobiński et al., (2010) and Dolnicki et al., (2013). A detailed description in the context of existing geophysical (ERT) and direct sampling results was given in the answer to Question 22.

Reference:

Glazer, M., Dobiński, W., Marciniak, A., Majdański, M., & Błaszczuk, M. (2020). Spatial distribution and controls of permafrost development in non-glacial Arctic catchment over the Holocene, Fuglebekken, SW Spitsbergen. *Geomorphology*, 358, 107128.

Dolnicki, P., Grabiec, M., Puczko, D., Gawor, L., Budzik, T., & Klementowski, J. (2013). Variability of temperature and thickness of permafrost active layer at coastal sites of Svalbard.

Dobiński, W., & Leszkiewicz, J. (2010). Active layer and permafrost occurrence in the vicinity of the Polish Polar Station, Hornsund, Spitsbergen in the light of geophysical research. *Problemy Klimatologii Polarnej*, 20, 129-142.

**32. Line 277.** “The early warning system can provide long-term tracking of permafrost conditions particularly when the ice content or mechanical properties of permafrost approach critical values.” What are the critical values? Again, either the concept of an early warning system should be developed fully and convincingly, or it should just be mentioned briefly as a goal for future

research efforts.

In the revised manuscript, we have clarified the application of early detection and warning systems to detect the presence of layers vulnerable to permafrost carbon feedback and emission of greenhouse gases into the atmosphere will be the goal of future study, as discussed in detail in the response to Question 4.

### 3 Technical corrections

1. It would be much easier to read if references to appendices were presented in the form “Appendix D” not simply “D” e.g., line 90 “the matrix... are given in D” would become “the matrices... are given in Appendix D”

We have revised this accordingly.

2. Line 17 “the active layer, may undergo seasonal thaw and freeze cycles” should be “the active layer, undergoes seasonal thaw and freeze cycles”

We have removed ‘may’ accordingly.

3. Line 29 “This distinction is determined by the amount of ice content within the permafrost.” Should be “This distinction is determined by the ice content within the permafrost.” OR “This distinction is determined by the amount of ice within the permafrost.”, amount and content both refer to the same quantity here.

We have revised this into ‘This distinction is determined by the ice content within the permafrost’.

4. Line 30 “Ice-rich permafrost contains ice in excess of its water content at saturation.” Could be modified to “Ice-rich permafrost contains ice in excess of its water content at saturation and is thaw unstable.” In order to improve the flow of argumentation in the surrounding paragraph.

We have revised this sentence into ‘Ice-rich permafrost contains ice in excess of its water content at saturation and is thaw unstable’.

5. Line 47 “GPR has been also used” should be “GPR has also been used”

This sentence has been revised into ‘GPR has also been used for mapping the thickness of the active layer’.

6. Line 50. “none of the above-mentioned methods characterizes the mechanical properties of permafrost layers.” Should rather be “none of the above-mentioned methods directly characterizes the mechanical properties of the permafrost.”

We have added ‘directly’ in this sentence.

7. Line 67. “based on an MASW seismic investigation in a field located at SW Spitsbergen, Norway” should rather be “based on a MASW seismic investigation of a field site located on SW Spitsbergen, Svalbard”.

We have added ‘site’ and replaced Norway with Svalbard.

8. Line 77. “A random sample is initially generated to ensure that soil parameters are not affected by a local minimum” makes it sound as if it is a single initial sample. I think the following might be a more correct representation of what the authors mean to express “A set of initial values, randomly selected and spanning the multidimensional parameter space ensures that soil parameters

are not affected by a local minimum". Same comment applies to line 123.

We have revised this sentence accordingly (A set of initial values, randomly selected and spanning the multidimensional parameter space ensures that soil parameters are not affected by a local minimum).

9. Figure 1 caption. "Dispersion relations of R1 and R2 waves" should be "Dispersion image of R1 and R2 waves". The annotation on figure panel (b) should also be changed since the figure shows dispersion images and not curves.

We have replaced 'relations' with 'image'.

10. Line 167. It is more geographically descriptive to write SW Spitsbergen, Svalbard (rather than Norway).

We have corrected this and replaced it with 'Svalbard'.

11. Line 169. Why not give the number of geophones directly? E.g. "The MASW test was performed by using 60 geophone receivers spaced at regular 2m intervals".

This sentence has been revised into: 'The MASW test was performed by using 60 geophone receivers with a frequency of 4.5 Hz spaced at regular 2 m intervals'.

12. Line 193. "detection of the thin ice lenses using low frequency seismic waves is highly impossible due to the mismatch between the thickness of the ice segregation layers and the wavelength generated in seismic tests". It is not valid to say "highly impossible". Why not simply say that ice lenses cannot be detected directly below  $1/4$  lambda, or whatever fraction of a wavelength is believed to be the correct detection limit here? To describe the phenomenon as a mismatch between wavelength and thickness is rather vague.

This sentence has been revised into 'The thin ice lenses can not be detected directly when the thickness of ice lenses is smaller than  $1/2$  wavelength generated by low frequency seismic waves'.

13. Line 201. "with a nearly 8.8%-22% of degree of saturation" it does not make sense to say nearly followed by a range, just give the range and omit "nearly".

We have removed 'nearly' accordingly.

14. Line 209. "sufficiently close" is a highly subjective description. "show good visual agreement" is perhaps what the authors intend to convey, but the phrasing should be made more descriptive in any case.

We have replaced it with 'show good agreement'. A root mean square value is also added to quantify the L2 distance between numerical predictions and experimental measurements.

15. Figures 5, 6, B1-B4 and line 258 in text "Saturation degree" should be "degree of saturation" which is the correct terminology and that which is mostly used throughout the text.

We have replaced it with 'degree of saturation' in those figures.